Primary Research Article – Revised Version

Podocalyxin and ciliary neurotrophic factor receptor are novel components of the surfaceome of chondrogenic cells

Patrik Kovács[1], Peter Brazda[2], Tibor Hajdú[1], Boglárka Harsányi[1], Krisztián Juhász[1], Roland Takács[1], Judit Vágó[1], Zhangzheng Wang[1], Clare Coveney[3], David J. Boocock[3], Csaba Matta[1,*]

[1] Department of Anatomy, Histology and Embryology, Faculty of Medicine, University of Debrecen, Debrecen, H-4032, Hungary
[2] Central for Translational Immunology, University Medical Center Utrecht, Utrecht University, Utrecht, The Netherlands
[3] School of Science and Technology, Nottingham Trent University, Nottingham NG11 8NF, United Kingdom

* To whom correspondence should be addressed. Tel: +36-52-255+567; Email: matta.csaba@med.unideb.hu

Running title: The Chondroprogenitor Surfaceome

ORCiD IDs:
Patrik Kovács: 0000-0003-1588-7962
Peter Brazda: 0000-0002-0215-1692
Tibor Hajdú: 0000-0002-9954-1987
Krisztián Juhász: 0009-0009-4299-3227
Roland Takács: 0000-0002-1598-3922
Judit Vágó: 0000-0003-4379-6734
Zhangzheng Wang: 0000-0003-3871-5143
Clare Coveney: 0000-0001-7047-6408
David J. Boocock: 0000-0002-7333-3549
Csaba Matta: 0000-0002-9678-7420

Abstract

Background: Osteoarthritis is a degenerative joint disease characterized by progressive loss of articular cartilage and limited capacity for intrinsic repair. A major barrier to developing effective regenerative strategies is the incomplete understanding of the molecular mechanisms regulating chondrogenesis and cartilage maintenance. Cell surface proteins are key mediators of extracellular communication, adhesion, and signaling, yet the chondrogenic surfaceome remains incompletely mapped, with prior studies focusing primarily on mature or cytokine-activated chondrocytes. The aim of this study was to provide a temporal profile of the surfaceome during *in vitro* chondrogenic differentiation and to identify novel membrane proteins with potential roles in cartilage biology.

Methods: We applied a sialoglycoprotein-targeted glycocapture strategy to selectively enrich plasma membrane proteins from chick embryonic limb bud-derived micromass cultures undergoing chondrogenesis. Enriched samples underwent high-resolution shotgun proteomic analysis, and differentially expressed candidates were validated by western blotting, immunocytochemistry, and transient gene silencing. Functional effects on extracellular matrix gene regulation were assessed by quantitative RT-PCR and matrix histochemistry.

Results: This approach generated the first temporal surfaceome map of chondrogenic progenitors. Among identified candidates, two proteins not previously linked to chondrogenesis, podocalyxin (PODXL) and ciliary neurotrophic factor receptor (CNTFR), were detected at the plasma membrane and confirmed at the protein and transcript levels. Both proteins exhibited time-dependent downregulation during differentiation. Targeted knockdown revealed differential regulation of the fibrocartilage marker *COL1A1* expression, indicating non-redundant roles in cell-matrix signaling and survival pathways. Single-cell transcriptomic meta-analysis confirmed expression of both proteins in discrete human articular chondrocyte subpopulations.

Conclusions: This study expands the molecular framework of chondrogenesis, identifying PODXL and CNTFR as novel, temporally regulated surfaceome components with distinct roles

in extracellular matrix signaling. These findings complement prior proteomic analyses of cytokine-activated mature articular chondrocytes and suggest new candidates for developmental cartilage biomarkers and therapeutic targets for osteoarthritis. Our results provide a resource for future cross-species surfaceome studies and highlight key pathways for further investigation into cartilage lineage specification and matrix adaptation.

(318 words in Abstract)

Plain English Summary

Osteoarthritis is the most common joint disease worldwide, causing pain, stiffness, and reduced mobility as the smooth cartilage that covers the ends of bones gradually breaks down. Cartilage has a very limited ability to heal itself, and there are currently no treatments that can stop or reverse the disease. Scientists are working on new ways to repair or replace damaged cartilage, but to do this effectively, they need to understand the molecular “language” that cartilage-forming cells use to develop and maintain healthy tissue.

In this study, we examined the set of proteins that are present on the surface of cartilage-forming cells, known as the “surfaceome.” These surface proteins play important roles in how cells connect to their surroundings, receive signals, and work together to build the cartilage matrix. Using a method to selectively capture and analyze these proteins, we discovered two that had never been linked to cartilage development: podocalyxin and ciliary neurotrophic factor receptor.

We found that these two proteins may have opposite effects on cartilage quality. Because they can be detected on the outside of cells, they could be developed into markers for early osteoarthritis detection or as targets for new therapies. Our findings open the door to new strategies for diagnosing and treating joint disease by focusing on cell-surface communication.

Keywords

surfaceome; chondrogenesis; cartilage regeneration; glycocapture; proteomics; cartilage; osteoarthritis; PODXL; CNTFR

Background

Osteoarthritis (OA) is the most common form of arthritis, characterized by the progressive degeneration of articular cartilage, subchondral bone sclerosis, synovial inflammation, osteophyte formation, and subsequent loss of joint function, leading to chronic pain and disability (1). OA imposes a substantial global health burden, affecting more than 303 million adults worldwide (2). Despite its high prevalence, there are currently no FDA-approved disease-modifying OA drugs capable of halting disease progression or promoting cartilage repair, largely due to the heterogeneous nature of OA and incomplete understanding of its molecular drivers (3). Current treatments remain palliative, focusing on symptom relief, underscoring an urgent unmet need for innovative therapeutic strategies (4).

Regenerative medicine has emerged as a promising avenue to address this gap. Stem cell-based approaches, particularly those using mesenchymal stem cells (MSCs), hold potential for cartilage regeneration and functional restoration (5). However, clinical outcomes have thus far been modest (6). The major obstacles include poor MSC survival in the inflammatory joint microenvironment, coupled with limited integration into native cartilage, which often result in transient improvements without sustainable extracellular matrix (ECM) restoration (2), (7). A deeper understanding of the molecular pathways that control chondrogenesis is therefore essential for improving cartilage repair outcomes (8).

A key step in this process is identifying novel biomarkers in chondroprogenitor cells that could provide mechanistic insight into cartilage differentiation, guide patient stratification in light of OA heterogeneity, and inform targeted regenerative strategies. Biomarkers predictive of chondrogenic capacity could significantly improve MSC-based cartilage repair by enabling optimal cell sourcing and enhancing survival, integration, and ECM restoration.

In this context, profiling the surfaceome, i.e., the full dynamic complement of cell surface proteins, is of particular importance for understanding chondroprogenitor cell biology and optimizing cartilage tissue engineering approaches (9-11). Current surface markers such as CD44, CD73 show variable association with the chondrogenic potential of MSCs derived from different tissues (12), highlighting the need for more reliable and functionally relevant

surface markers (13). Such biomarkers could not only improve the selection of optimal cell types for therapy but also support the design of biomaterials that mimic native chondrogenic niches (14).

Our group has previously performed sialoglycoprotein-based surfaceome mapping of mesenchymal stem cells and migratory chondrogenic progenitor cells to define adhesive and signaling signatures at early cartilage lineage commitment, and to highlight differences between these two cell types (9). In a subsequent study, we used a similar approach on primary equine articular chondrocytes under normal and pro-inflammatory conditions to reveal cytokine-induced surfaceome remodeling (15). While such earlier work has defined features of the chondrocyte surfaceome under various physiological and pathological conditions, there is a need for systematic temporal analysis during chondrogenic differentiation. Therefore, by building on earlier findings, we aimed to establish a temporal, quantitative map of the chondrogenic surfaceome using a developmental *in vitro* model to identify new membrane-associated proteins involved in cartilage differentiation and phenotype stabilization.

Here, we present a temporal landscape of the surfaceome of chondrogenic progenitor cells during chondrogenesis. Using a sialoglycoprotein-targeted glycocapture method with aminooxy-biotin, followed by shotgun proteomics (9, 15, 16), we enriched the cell surface subproteome. We aimed to determine which membrane-associated proteins may be associated with the transition from chondroprogenitor to mature chondrocyte states and how these proteins integrate with extracellular matrix and cell-survival signaling. We identified proteins not previously linked to chondrogenic differentiation. Notably, we discovered podocalyxin (PODXL), a sialomucin known for regulating podocyte polarity, and ciliary neurotrophic factor receptor (CNTFR), a neurotrophic signal transducer, as novel constituents of the chondrogenic surfaceome. Their detection suggests convergence of adhesion- and survival-related signaling pathways during chondrogenesis, expanding current knowledge of extracellular signaling in cartilage development and highlighting potential translational targets for OA therapy.

148 **Methods**

149 *1. Experimental setup*

150 This study employed a staged approach to define the surfaceome of embryonic
151 chicken limb bud-derived chondrogenic cells at key stages of chondrogenic differentiation.
152 Temporal proteomic profiling was conducted at days 1, 3, 6, 10, and 15 of micromass culture
153 corresponding to key histodifferentiation stages (17, 18), combining sialoglycoprotein
154 enrichment via aminooxy-biotin conjugation with high-resolution LC-MS/MS on 3 biological
155 replicates (N = 3). Candidate surface markers ciliary neurotrophic factor receptor (CNTFR)
156 and podocalyxin (PODXL) were validated through RT-qPCR, western blotting, and
157 immunocytochemical localization. The integrated workflow, spanning discovery to functional
158 validation, is summarized in Figure 1.

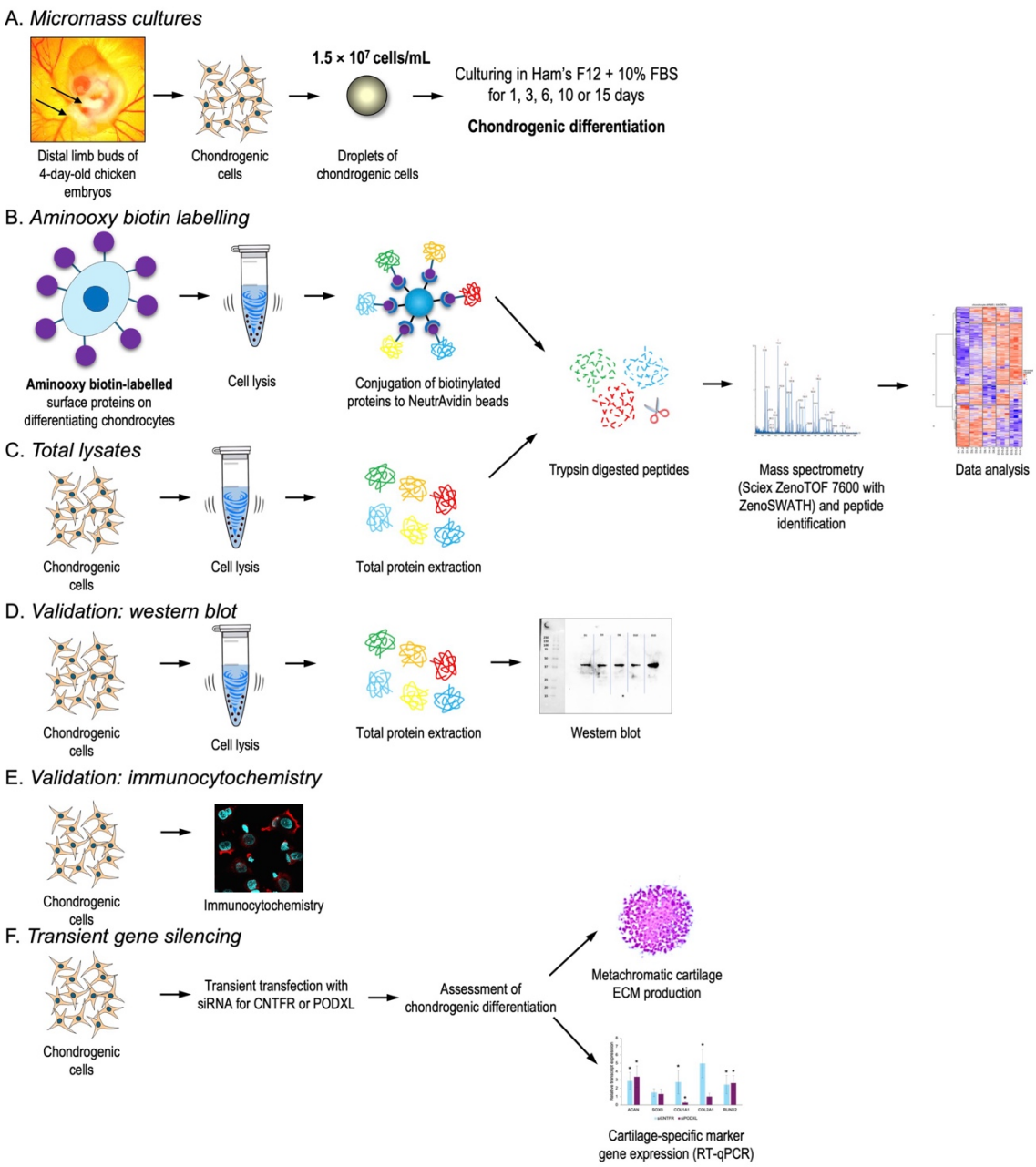

Figure 1. Experimental workflow.

2. Chondrogenic micromass cultures

Chondrogenic micromass cultures were established from embryonic chicken limb bud chondroprogenitors using a standardized protocol optimized for spontaneous chondrogenesis (18). Briefly, distal parts of limb buds were carefully excised from early-stage (Hamburger–Hamilton 22–24) chicken embryos and dissociated into a single-cell suspension via trypsin-EDTA digestion. Cells were resuspended in Ham's F12 medium (Gibco, Thermo Fisher

168 Scientific) supplemented with 10% fetal bovine serum (FBS, Gibco) and plated as 100 µL
169 micromass droplets (1.5 × 10^7 cells/mL) onto 6-well plates. Following a 2-hour adhesion phase
170 (37°C, 5% CO_2), cultures were gently flooded with fresh medium to maintain 3D architecture.
171 This model recapitulates *in vivo* chondrogenesis, including *COL2A1* upregulation and *SOX9*-
172 dependent ECM synthesis, as previously characterized in this system (17, 18). Cultures were
173 harvested at days 1, 3, 6, 10, and 15 to capture key transitions in surfaceome dynamics during
174 early differentiation.
175
176 *3. Cell surface proteome labelling and enrichment, and total cell lysates*
177 For a detailed methodology for cell surface sialoglycoprotein labelling and enrichment
178 of chondroprogenitor cells in micromass cultures, please see our protocol paper (16). Unless
179 otherwise stated, all reagents were purchased from Thermo Fisher Scientific. Briefly, sialic
180 acid residues on the cell surface proteins of micromass cultures were oxidized using 1 mM
181 sodium meta-periodate to generate reactive aldehyde groups. This was followed by incubation
182 in the dark for 1 hour at 4°C with 100 mM aminooxy-biotin (Biotium). After quenching with
183 glycerol, the labelled cells were lysed (1% Triton X-100, 150 mM NaCl, 5 mM iodoacetamide,
184 10 µL protease inhibitor cocktail, 0.1 mg/mL PMSF and 10 mM Tris-HCl; pH 7.6). Biotinylated
185 proteins were affinity-purified using NeutrAvidin agarose beads, followed by stringent washes
186 to remove nonspecific binders. Captured protein were reduced by 100 mM DTT and alkylated
187 in 50 mM iodoacetamide, and further wash steps were performed to minimize contamination
188 from intracellular components, and to prepare the sample for LC-MS/MS analysis. Captured
189 proteins were digested overnight with 5 µg MS-grade trypsin in 50 mM NH_4HCO_3. Solvents
190 were then evaporated in a vacuum concentrator centrifuge and stored at –80°C.
191 Parallel total proteome analysis of micromass cultures were prepared using lysis in
192 RIPA and sonication to shear DNA (3 × 10 sec pulses), ensuring membrane protein
193 solubilization. Samples were then stored at –80°C. This approach enabled comparative
194 quantification of surface-enriched vs. intracellular proteins during chondrogenesis.
195

196 *4. Mass spectrometry, protein identification and quantification*

197 Dried peptide samples were reconstituted in 150 µL of 10% acetonitrile with 0.1%
198 formic acid, shaken at 5°C for 20 minutes, followed by addition of 150 µL 0.1% formic acid to
199 yield a final concentration of 5% acetonitrile and 0.1% formic acid. After centrifugation at
200 12,000 × g for 2 minutes to remove particulates, supernatants were transferred to LC-MS
201 compatible vials. Peptide separation was performed on a Waters M-Class UPLC system
202 equipped with a Phenomenex Kinetex XB-C18 column (2.6 µm, 15 × 0.3 mm) maintained at
203 30°C, using a linear gradient of 3–35% acetonitrile (mobile phase B) over 12 minutes at a flow
204 rate of 10 µL/min, followed by washing at 80% B and re-equilibration to 3% B. Three microlitres
205 of each sample were injected in direct inject mode. Mass spectrometric analysis was
206 conducted on a Sciex 7600 ZenoTOF operating in positive ion mode with Data Independent
207 Acquisition (DIA, zenoSWATH), employing a 25 ms TOF-MS scan and 65 variable SWATH
208 windows (12 ms each) covering m/z 400–750, with a total cycle time of 1.146 s. Raw data files
209 were processed using DIA-NN (version 1.8.1) (19), with a *Gallus gallus* UniProt FASTA
210 database (Oct 2021), enabling library-free search and deep learning-based spectra prediction.
211 Label-free quantification was performed at a precursor false discovery rate (FDR) of 1.0%,
212 with default DIA-NN parameters unless otherwise specified. Protein identification and
213 quantification results were exported, and proteins were annotated using Gene Ontology (GO)
214 information from UniProt to infer subcellular localization (16).

215 The mass spectrometry proteomics data have been deposited to the
216 ProteomeXchange Consortium *via* the PRIDE partner repository with the dataset identifier
217 PXD064013.

218

219 *5. Bioinformatics and pathway analysis*

220 Proteomic intensity data were log2-transformed. Missing values were imputed using a
221 left-censored normal distribution via the minProb method (q = 0.001) from the *promor* package
222 in R (20) to simulate low-abundance signals below the detection threshold. Entries
223 representing protein families (where individual proteins could not be reliably deconvoluted)

224 were excluded from the downstream bioinformatic analysis workflow, as some of these were
225 also present as single entries in the matrix. Principal component analysis (PCA) was used to
226 assess sample variability and potential batch effects.

227 Differential protein expression (DEP) analysis was performed using the *DEqMS*
228 package in R, applying linear modeling with variance moderation based on peptide counts.
229 Proteins with |log2 fold-change| > 1 and Benjamini-Hochberg adjusted p-value (FDR) < 0.05
230 were considered DEPs. The *gorth* package was used to perform ortholog mapping from
231 chicken (*Gallus gallus*) to human (*Homo sapiens*). The resulting set of DEPs was z-score
232 scaled and grouped using hierarchical clustering to identify temporal expression patterns.

233 Gene Ontology (GO) enrichment analysis was performed for each DEP list and
234 temporal DEP cluster using *enrichGO*() and *compareCluster*() (*org.Hs.eg.db*, p-value < 0.05,
235 q-value < 0.2), covering Biological Process (BP), Molecular Function (MF), and Cellular
236 Component (CC) categories. Statistical analysis and visualization were carried out in R.

237 Our NGS dataset (BioProject IDs: PRJNA817177; PRJNA938813) (17) was processed
238 using R. Weighted gene correlation network analysis (WGCNA) was performed with the
239 *WGCNA* R package. For the construction of the protein-protein interaction (PPI) network, we
240 utilized the STRING database, and Cytoscape was employed to further screen the proximal
241 associated proteins. Enrichment analysis was carried out using the *clusterProfiler* R package.
242

243 *7. Immunocytochemistry*

244 On specified culture days, cells were dissociated using mild collagenase type I
245 treatment (Sigma) for 30 minutes at 37°C, resuspended in fresh F12 medium, and seeded
246 onto glass coverslips in 24-well plates. Cells were allowed to adhere for 2 hours in a humidified
247 incubator (37°C, 5% CO_2). Following attachment, cells were fixed in 10% formalin in 1 × PBS
248 for 30 minutes at room temperature (RT). After washing in PBS, non-specific binding sites
249 were blocked with 3% bovine serum albumin (BSA) and 10% serum from the host species of
250 the secondary antibody (see below) in PBS for 1 hour at RT.

251 For immunostaining, cells were incubated overnight at 4°C with anti-CNTFR (Abcam;
252 Cat. No. ab127425) at a dilution of 1:500, and anti-PODXL (Proteintech; Cat. No. 18150-1-
253 AP) antibodies at a dilution of 1:500, diluted in blocking solution. Primary antibodies were
254 detected using a goat anti-rabbit IgG secondary antibody conjugated to Alexa Fluor 555 (Life
255 Technologies Corporation; Cat. No. A27039) at a dilution of 1:1000, incubated for 1 hour at
256 RT. Cultures were mounted in Vectashield Hard Set mounting medium (Vector Laboratories)
257 containing DAPI to visualize nuclei. Subcellular localization of PODXL and CNTFR was
258 analyzed using an Olympus FV1000S confocal microscope (Olympus) equipped with a 60×
259 oil immersion objective (NA: 1.3). For excitation of AlexaFluor 555, 543 nm laser line was
260 used. The average pixel dwell time was 4 μs. Images of Alexa Fluor 555 and DAPI were
261 overlaid.
262
263 *8. Western blot analysis*
264 Total cell lysates for SDS–PAGE were prepared as previously described (21). To
265 ensure equal protein loading, after protein concentrations were determined, four-fold
266 concentrated Laemmli buffer (Thermo Fisher Scientific) was added to the lysates, and
267 samples were heated at 95°C for 10 minutes. In each lane, 20 μg of protein per sample was
268 loaded onto 10% SDS–polyacrylamide gels for separation. Following electrophoresis, proteins
269 were transferred onto nitrocellulose membranes using electroblotting. Membranes were
270 blocked with 5% non-fat dry milk dissolved in PBS for 1 hour at RT. Subsequently, membranes
271 incubated overnight at 4°C with the primary antibodies (anti-CNTFR at a dilution of 1:500, and
272 anti-PODXL at a dilution of 1:500). After three washes in PBST (PBS containing 0.1% Tween-
273 20) for a total of 30 minutes, membranes were incubated with an anti-rabbit IgG secondary
274 antibody (Bio-Rad Laboratories) in 1:1000 dilution for 1 hour at RT. Protein bands were
275 visualized using enhanced chemiluminescence (Millipore) according to the instructions
276 provided by the manufacturer. Equal protein loading was verified by probing for β-actin as a
277 loading control.
278

279 *9. Transient gene silencing of CNTFR and PODXL*

280 To investigate the impact of transient gene silencing of *CNTFR* and *PODXL* on
281 chondrogenic differentiation, freshly isolated limb bud-derived progenitor cells were
282 transfected with siRNA. Cells were resuspended at a density of 1.5×10^7 cells/mL in Ham's
283 F12 medium and seeded into 12-well plates. Custom-designed siRNAs targeting
284 CNTFR (Silencer™ Custom Designed siRNA; Cat. No. 4399666, Design ID: ABD1VPK) and
285 PODXL (Design ID: ABHSP78), along with a non-targeting (NT) control (Silencer™ Select
286 Negative Control No. 1 siRNA; Cat. No. 4390844; Life Technologies), were transfected into
287 chondrogenic cells 2 hours post-attachment using Lipofectamine™ RNAiMAX Transfection
288 Reagent (Cat. No. 13778150; Life Technologies) and Opti-MEM™ Reduced Serum
289 Medium (Cat. No. 51985034; Life Technologies).

290 For the analysis of cartilage ECM production following gene silencing, colonies were
291 fixed on culture day 6, stained with DMMB (pH 1.8), and photographed. Cartilage ECM
292 production was quantified using a MATLAB script (18), with values normalized to NT control
293 levels. Relative cell numbers or viability (inferred from mitochondrial activity) were analyzed
294 via MTT assay (18). Optical density values were expressed as percentage changes relative
295 to NT control.

296 Gene expression profiling of chondrogenic marker genes was performed as described
297 previously (17) with minor adjustments. Micromass cultures were harvested 48 hours post-
298 transfection. As cartilage ECM accumulation generally requires several days beyond this initial
299 time point, these assays were designed to capture transcriptional trends reflecting early
300 modulatory effects on chondrogenic gene regulation rather than fully developed phenotype
301 changes. Total RNA was isolated using TRI Reagent (Applied Biosystems) following to the
302 manufacturer's instructions. Total RNA (1 µg) was reverse-transcribed into cDNA using the
303 High-Capacity cDNA Reverse Transcription Kit (Thermo Fisher Scientific) according to the
304 manufacturer's protocol. The expression patterns of chondrogenic marker genes were
305 quantified via CYBR Green-based RT-qPCR using the $2^{-\Delta\Delta Ct}$ method. Primer sequences
306 (Integrated DNA Technologies) are provided in Table S1 (Additional file 1). RT-qPCR

307 reactions were set up using GoTaq qPCR Master Mix (Promega) and 20 ng of input cDNA per
308 each 10-μL reaction. Reactions were run on a QuantStudio 3 System (Thermo Fisher
309 Scientific) using a standard thermal profile (17). Of the six reference genes evaluated for
310 stability (*HPRT1*, *PPIA*, *RPL4*, *RPL13*, *RPS7*, *YWHAZ*), BestKeeper (22) identified *RPS7* as
311 the most stable transcript. All target gene data were normalized to *RPS7* expression.
312

313 **Results**

314 *1. Temporal proteome dynamics in chondrogenic cultures*

315 Principal component analysis (PCA) performed on the 5,207 proteins/protein groups
316 identified in total lysates from chondrogenic micromass cultures revealed distinct proteomic
317 profiles at each differentiation stage, with biological replicates clustering tightly by culture day
318 (Figure 2A–B). The first principal component (PC1), which explains 42% of the variance,
319 captured temporal progression, separating undifferentiated (day 1) from differentiated (days
320 10 and 15) cultures. PC2 (19% variance) distinguished intermediate differentiation stages
321 (days 3–6) from both early and late time points.

322 A total of 792 proteins (323, 159, 272, and 38 for each consecutive timepoint
323 comparison: day 1–3, day 3–6, day 6–10, and day 10–15, respectively) were identified as
324 significantly upregulated. Similarly, 1368 proteins (714, 231, 178, and 245 for each
325 corresponding timepoint comparison) were identified as significantly downregulated (Figure
326 S1 in Additional file 1). Full lists of differentially expressed proteins (DEPs) for pairwise
327 comparisons between consecutive days and between undifferentiated (day 1) versus mature
328 (day 15) cultures are provided in the Supporting Information (Additional file 2).

329 To better characterize DEPs between each time point, we performed gene ontology
330 (GO) analysis on the DEPs (Figure 2C–D). In case of proteins that were upregulated in
331 consecutive time points, GO terms related to collagen-containing ECM synthesis, ECM
332 organization, and integrin binding were over-represented. In contrast, when we looked at the
333 downregulated DEPs separately, a much broader range of GO terms were identified, such as
334 those related to DNA and RNA metabolism, DNA replication, and transcription factor binding,
335 especially in the earlier time points. Between days 10–15, ECM-related GO terms were also
336 enriched, indicating that ECM production has been completed by day 15 (mature/hypertrophic)
337 cultures.

338

339

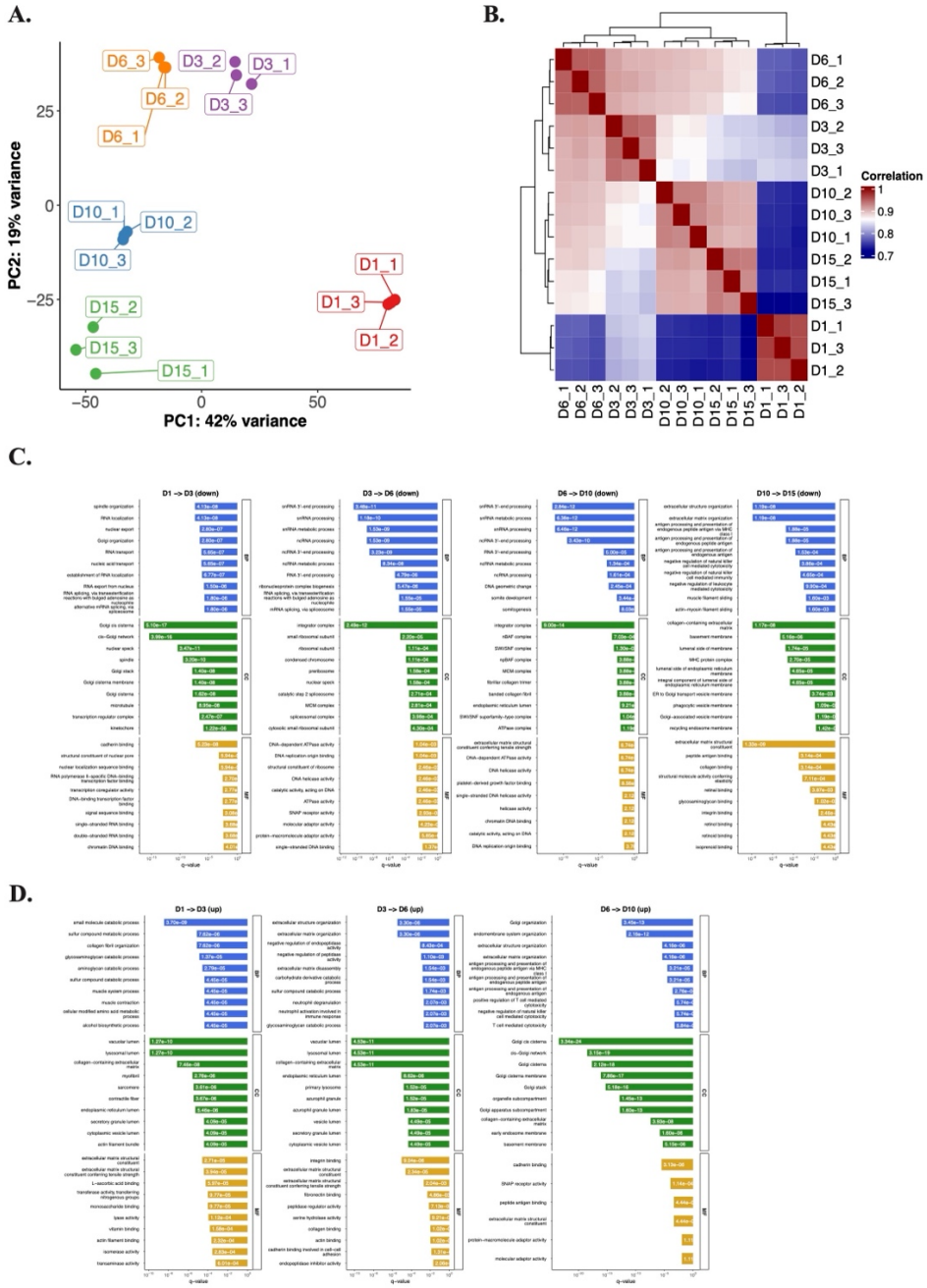

Figure 2. Quantitative proteomics analysis of total cell lysates from chondrogenic micromass cultures. A. Principal component analysis (PCA) of the total lysate samples of micromass cultures of chondroprogenitor cells undergoing chondrogenesis (5,207 proteins in the entire dataset). Each dot represents a biological replicate (n = 3). The PCA plot shows unsupervised clustering according to culture age along the principal component (PC) 1 and PC2 hyperplanes, accounting for 42% and 19% of the variance, respectively. **B.** The correlation matrix also demonstrates clear separation among the samples according to culture age. **C–D.** Enrichment analysis using gene ontology (GO) annotations for pairwise comparisons of culture days, showing the top GO terms (biological process (BP), cellular compartment (CC), or molecular function (MF)) by ranking them by the adjusted p-values (p.adjust < 0.001). Plots shown separately for upregulated (**C**, top panel) and downregulated (**D**, bottom panel) proteins. The *x*-axis is the adjusted p-value of the enriched terms.

353 *2. Representative proteins and pathways in chondrogenic cultures*

354 The identified DEPs in the total lysates of chondrogenic cultures were categorized into
355 5 clusters to delineate expression dynamics (Figure 3A–B). Protein lists for each cluster are
356 provided in the Supporting Information (Additional file 3).

357 **Cluster 1** (625 proteins) exhibited an initial steep downregulation during early *in vitro*
358 chondrogenesis (days 1–3), plateauing thereafter. This group showed enrichment for GO
359 terms related to RNA splicing, histone acetyltransferase activity, and RNA polymerase II
360 mediated transcription (Figure 3C), suggesting phased suppression of transcriptional
361 machinery in maturing cultures. Key proteins in this group include AKT1, FN1, SOX5,
362 NOTCH1, and ITGB1. AKT1 is a central component in the PI3K/Akt pathway, which modulates
363 the balance between chondrocyte proliferation and differentiation (23). Fibronectin (FN1), an
364 ECM glycoprotein, drives chondrocyte differentiation and collagen production via the PI3K/Akt
365 signaling pathway (24). The SOX5 transcription is part of the SOX trio (SOX5, SOX6, SOX9)
366 driving chondrogenic lineage commitment and promoting expression of key cartilage ECM
367 genes such as *COL2A1* (25). NOTCH1 is a receptor that regulates early chondrogenic lineage
368 differentiation via SOX9 (26). Integrin beta-1 (ITGB1) is a cell surface receptor that mediates
369 cell–matrix adhesion and signals for chondrocyte proliferation, migration, and differentiation
370 (27).

371 **Cluster 2** (173 proteins) displayed peak expression at day 6, with overrepresented GO
372 terms linked to amino acid metabolism, connective tissue development, and collagen
373 synthesis. This cluster included several functionally relevant proteins outside the collagen
374 family (such as COL1A1, COL5A1, COL12A1, COL14A1, COL15A1), notably FRZB,
375 TGFBR2, NFATC1, and THBS2, all of which are recognized as being involved in chondrocyte
376 phenotype regulation, matrix remodeling, growth factor signaling, and cartilage regeneration.
377 Specifically, frizzle-related protein (FRZB) is a secreted Wnt agonist that maintains
378 chondrocyte phenotype and is highly expressed in articular chondrocytes (28). Transforming
379 growth factor beta receptor II (TGFRB2), a cell surface receptor, is a critical regulator of
380 chondrocyte maturation, and is essential in maintaining cartilage integrity (29). Nuclear factor

of activated T-cells 1 (NFATC1) is a transcription factor that acts as a marker in articular cartilage progenitor cells. It is a key mediator of chondrocyte fate (30). Thrombospondin 2 (THBS2) is an ECM glycoprotein involved in cartilage regeneration (31).

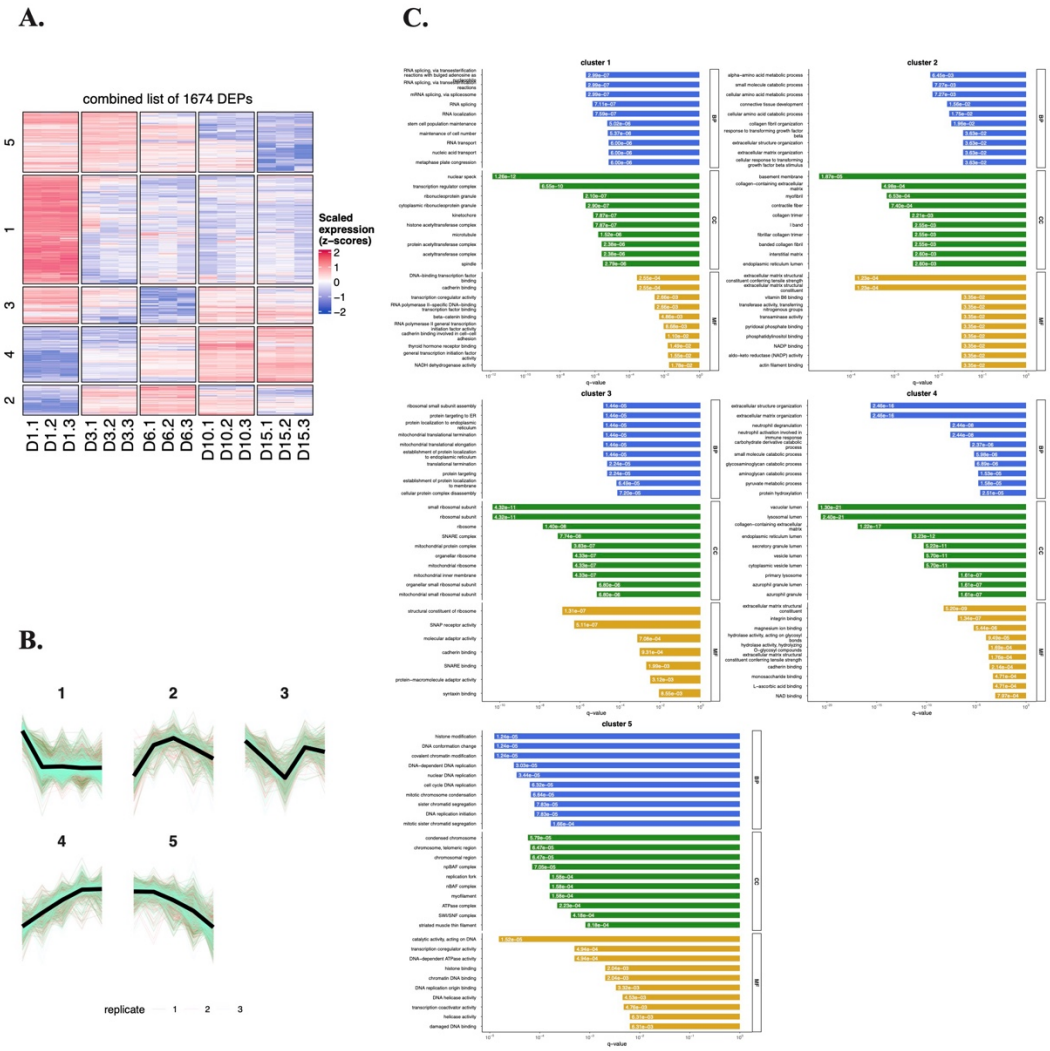

Figure 3. Unsupervised clustering analysis of differentially expressed proteins (DEPs) in total cell lysates of chondrogenic cultures using the k-means algorithm. A–B. The expression dynamics of each cluster are shown in clusters 1–5. *x*-axis, time points (days of culturing). **C.** Pathway analysis using Gene Ontology (GO) annotation for the 5 clusters of proteins in total lysates of chondrogenic cells undergoing chondrogenic differentiation. Select terms for GO biological process (BP), cellular component (CC), and molecular functions (MF). Barplot shows significant terms, the *x*-axis is gene (protein) ratio and the number of proteins belonging to given enriched terms. These clusters outline a progressive remodeling of the proteome from a proliferative, transcriptionally active progenitor profile toward an ECM-producing, metabolically adapted chondrocyte phenotype.

Cluster 3 (211 proteins) followed a U-shaped trajectory: downregulated initially but upregulated in later stages and was enriched for GO terms related to mitochondrial and ribosomal functions. This cluster contained key signaling and matrix-interacting proteins,

398 including ACVR1 (BMP receptor required for chondrogenesis), decorin (DCN), syndecan-1
399 (SDC1), tenascin-C (TNC), and transferrin receptor (TFRC), all of which have mechanistic
400 roles in regulating chondrocyte proliferation, differentiation, matrix integrity, and
401 developmental signaling in cartilage tissue (32, 33). Notably, decorin is a proteoglycan in the
402 cartilage pericellular and territorial matrix that regulates ECM architecture and load-bearing
403 properties (34). Syndecan-1 is a cell-surface protepglycan involced in cell–matrix interactions
404 (35). Tenascin-C is an ECM glycoprotein with important roles in cartilage development and
405 ECM production (36).

406 **Cluster 4** (319 proteins) demonstrated progressive upregulation, peaking in mature
407 chondrocytes (days 10–15), suggesting that these proteins are associated with the later
408 stages of chondrogenic differentiation and may contribute to the functional maturation of
409 chondrocytes. Over-represented GO terms in this cluster were related to ECM and collagen
410 synthesis. This cluster included classic and emerging modulators of cartilage ECM and
411 chondrocyte function such as ACAN (aggrecan, the major cartilage proteoglycan), major
412 collagen types (COL2A1, COL6A1, COL8A1, COL9A1, COL22A1), COMP (cartilage
413 oligomeric matrix protein; involved in matrix assembly), MATN1 (matrilin-1; involved in
414 mechanotransduction), TIMP3 (tissue inhibitor of metalloproteinases; involved in matrix
415 protection), ENO1 (alpha-enolase; involved in glycolysis) and LDHA (lactate dehydrogenase;
416 involved in chondrocyte-specific glycolytic adaptation), all vital for cartilage tissue integrity and
417 repair (8, 37).

418 **Cluster 5** (346 proteins) showed a similar expression pattern to cluster 1 but with a
419 more sustained downregulation throughout chondrogenesis. Over-represented GO terms in
420 this cluster included histone modification and cell proliferation (DNA replication and
421 chromosome condensation). This cluster included functional components and matrix
422 regulators such as CD44 (hyaluronan adhesion), PDGFRA (platelet-derived growth factor
423 receptor alpha; essential for chondroprogenitor specification), FBN2 (fibrillin-2; involved in
424 matrix assembly and growth factor regulation), and VCAN (versican; modulates cartilage

425 morphogenesis and growth factor localization), all implicated in cartilage and joint
426 development, repair, or disease (38-41).
427 Next, we carried out a detailed protein-protein interaction (PPI) analysis of each cluster
428 using STRING and generated a small network with the top 20 hub proteins (Figure S2). In the
429 PPI network of **Cluster 1**, spliceosome and ribosome biogenesis are recurrent pathways.
430 Components of the PI3K/Akt and Wnt signaling were also enriched, whereas BIRC5 and
431 SUMO1 regulate apoptosis and post-translational modifications, respectively. The PPI
432 network in **Cluster 2** is centrally enriched in ECM dynamics and cell–matrix signaling, with
433 focal adhesion and PI3K/Akt as hub pathways. The proteins in the network of **Cluster 3** are
434 predominantly associated with ribosomal biogenesis, translation, and RNA processing, with
435 strong enrichment in conserved pathways such as global protein synthesis, protein processing
436 in endoplasmic reticulum, and mitochondrial translation. In a similar way to Cluster 2, the PPI
437 network of **Cluster 4** is enriched in ECM remodeling, glycolysis, and cell adhesion signaling.
438 ECM dynamics dominate this cluster, with collagens and modifiers driving ECM integrity.
439 Glycolysis enzymes highlight metabolic reprogramming, and focal adhesion and PI3K/Akt
440 couple signaling to pro-survival pathways. For **Cluster 5**, the PPI network is enriched in cell
441 cycle regulation, DNA replication/repair, and chromatin remodeling.
442
443 *3. Chondrogenic surfaceome dynamics via aminooxy-biotin enrichment*
444 We next profiled the surfaceome during chondrogenic differentiation. Of 522 quantified
445 proteins/protein groups, 18 detected in only one time point were excluded, leaving 504
446 proteins for differential protein expression analysis. PCA revealed low degree of variability
447 among biological replicates, with clear separation by culture day along PC1 (40% variance)
448 (Figure 4). This trajectory mirrored trends observed in the total proteome, reflecting stage-
449 specific surfaceome dynamics as cells progressed from undifferentiated (day 1) to mature (day
450 15) states.
451

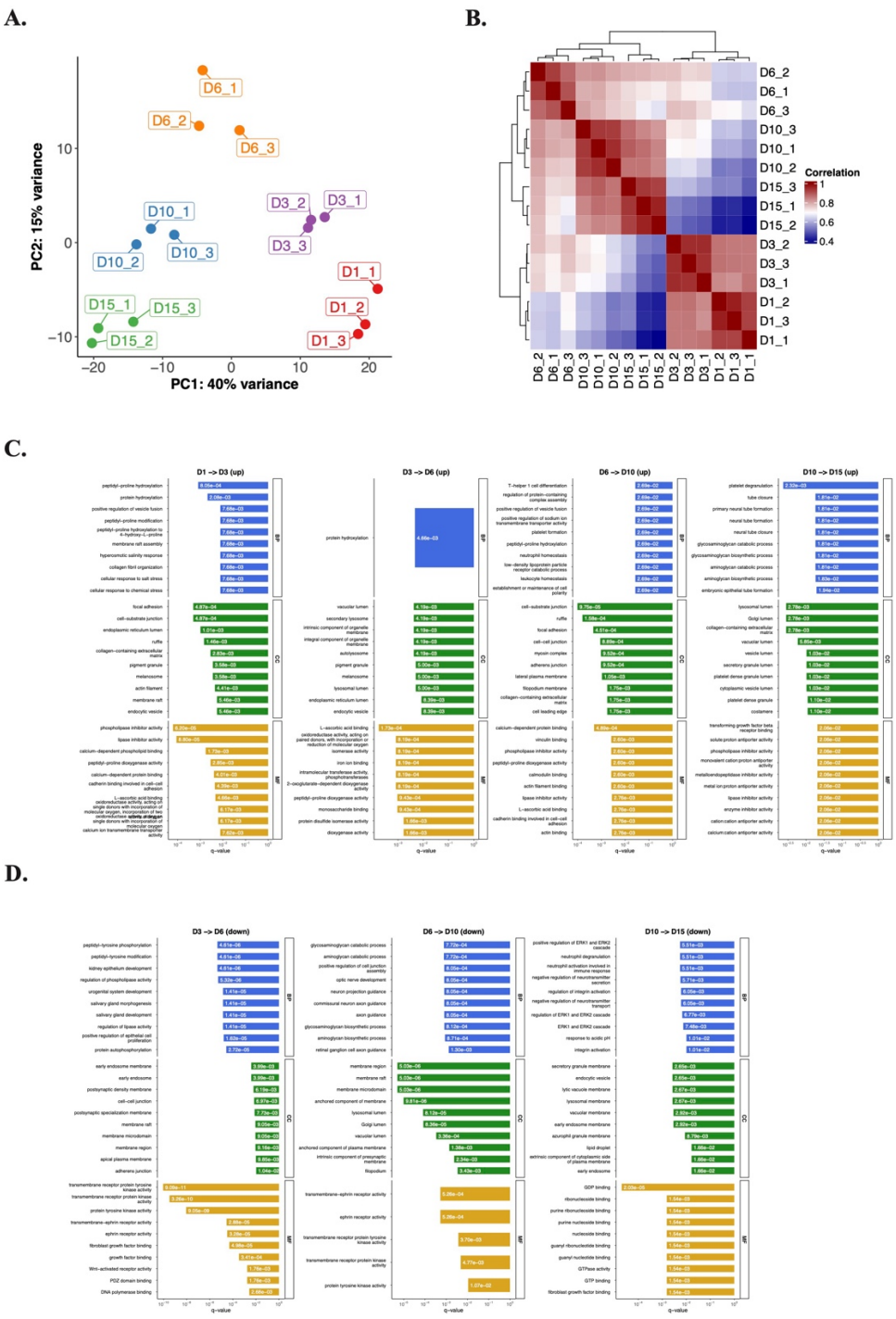

Figure 4. Quantitative proteomics analysis of aminooxy biotin (AOB) enriched samples from chondrogenic micromass cultures. A. PCA of the AOB-enriched samples of micromass cultures undergoing chondrogenesis (504 proteins in the dataset). Each dot represents a biological replicate (n = 3). The samples clustered together according to culture age along the principal component (PC) 1 and PC2 hyperplanes, which account for 40% and 15% of the variance, respectively. **B.** The correlation matrix (right panel) also signifies separation among the samples according to differentiation status. **C–D.** Pathway analysis using Gene Ontology (GO) annotation for the AOB-enriched subproteome of chondrogenic cells undergoing chondrogenic differentiation. Panel shows the top GO terms based on biological process (BP), cellular compartment (CC), or molecular function (MF), separately for upregulated (**C**, top panel) and downregulated (**D**, bottom panel) proteins, following ranking by adjusted p-values. The *x*-axis is the adjusted p-value of the enriched terms.

464 A total of 254 proteins (72, 74, 89, and 19 for each consecutive timepoint comparison:
465 day 1–3, day 3–6, day 6–10, and day 10–15, respectively) were identified as significantly
466 upregulated. Similarly, 170 proteins (10, 82, 31, and 47 for each corresponding timepoint
467 comparison) were identified as significantly downregulated (Figure S3). DEP lists for pairwise
468 comparisons of subsequent culture days are provided in the Supporting Information
469 (Additional file 4).

470 We performed GO analysis on DEPs that were up or downregulated in later time points
471 to better characterize DEPs between each time point (Figure 4C–D). Upregulated proteins
472 were enriched in collagen biosynthesis (terms such as peptidyl-prolyl hydroxylation, L-
473 ascorbic acid binding), ECM maturation (glycosaminoglycan biosynthesis), and cell–matrix
474 adhesion, consistent with chondrocyte functional specialization. In contrast, GO terms
475 associated with downregulated DEPs included developmental signaling (ephrin receptor
476 pathway, Wnt-activated receptor activity, regulation of ERK1 and ERK2 cascade), growth
477 factor modulation, and several terms related to neural processes (synapses and axonal
478 growth), suggesting attenuation of plasticity pathways in mature cells.

479

480 *4. Representative proteins and pathways in the chondrogenic surfaceome*

481 Proteins in the aminooxy-biotin-enriched subproteome were classified into four
482 clusters based on expression dynamics (Figure 5A–B). Protein lists for each cluster are
483 provided in the Supporting Information (Additional file 5).

484 **Cluster 1** (96 proteins) exhibited progressive upregulation during *in vitro*
485 chondrogenesis, enriched in GO terms such as ECM organization, L-ascorbic acid binding,
486 and peptidyl-prolyl hydroxylation (related to collagen alpha-chain synthesis), and bone
487 development (Figure 5C). In addition to an overrepresentation of collagens, surfaceome
488 cluster 1 contains key chondrocyte regulators and cartilage matrix constituents including
489 MATN1 (pericellular mechanotransduction), SDC4 (syndecan-4; involved in ECM signaling),
490 EPYC (epiphycan; a proteoglycan modulating collagen fibrillogenesis), TRPV4 (transient

receptor potential vanilloid 4; involved in mechanosensation), and SFRP3 (secreted frizzled-related protein 3; a Wnt pathway inhibitor), together highlighting its biological significance for cartilage phenotype maintenance and differentiation (42-44).

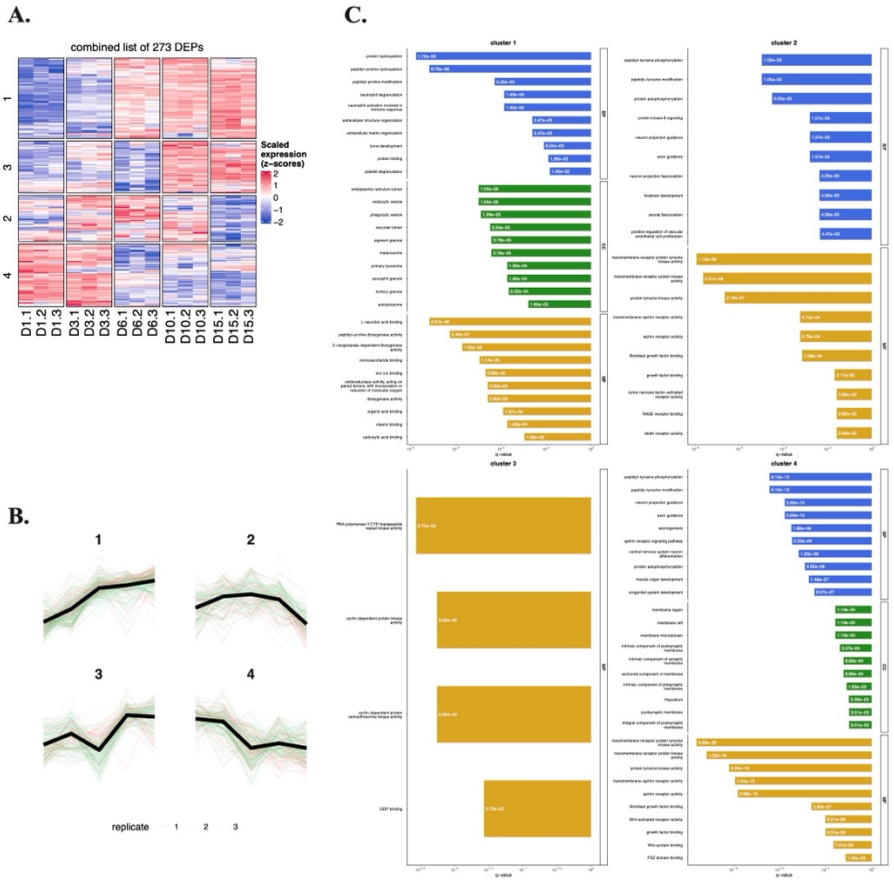

Figure 5. Unsupervised clustering analysis of differentially expressed proteins in the AOB-enriched subproteome during chondrogenesis using the k-means algorithm. A–B. The expression dynamics of each cluster are visible in clusters 1–4. The *x*-axis represents the time points (days of culturing). **C.** Pathway analysis using Gene Ontology (GO) annotation for the 4 clusters. Selected terms for GO biological processes (BP), cellular component (CC), and molecular functions (MF). Barplot shows significant terms, the *x*-axis is gene (protein) ratio and the number of proteins belonging to given enriched terms. Together, these clusters outline the progressive remodeling of the chondrogenic surfaceome.

Cluster 2 (60 proteins) showed peak expression on culture day 6, with overrepresented GO terms such as kinase activity, ephrin receptor activity, growth factor binding, and FGF signaling. Surfaceome cluster 2 harbors several cell-surface regulators of chondrocyte biology, including RECK (a membrane-anchored matrix metalloprotease inhibitor (45)), FGFR2 (fibroblast growth factor receptor 2; regulates chondrocyte

509 proliferation/differentiation signaling (46)), multiple ephrin receptors (EPHA7, EPHB2, EPHB1,
510 EPHB3 with potential roles in cartilage morphogenesis (47)), SRC kinase (chondrocyte
511 phenotype control (48)), and GPC1 (glypical-1; a proteoglycan and cell surface co-receptor
512 involved in growth factor pathway modulation (49)), highlighting surfaceome mechanisms in
513 cartilage development and regeneration.

514 **Cluster 3** (63 proteins) displayed transient suppression on culture day 6, followed by
515 late-stage upregulation in mature cultures, with overrepresented GO terms related to RNA
516 polymerase II and the cell cycle. This cluster includes surfaceome and secreted proteins with
517 established contributions to cartilage biology, such as FGFR3 (regulation of proliferation and
518 differentiation (50)), TGFR2 (matrix synthesis and hypertrophy control), TIMP3 (matrix
519 protection), TSP2, and ANXA1 (annexin A1; chondroprotection and matrix homeostasis (51)),
520 together highlighting the complexity of chondrocyte surface signaling and matrix regulation

521 **Cluster 4** (88 proteins) declined steadily after day 3 in mature chondrocytes,
522 suggesting roles restricted to early differentiation. Enriched GO terms in this cluster include
523 muscle and nervous system development, as well as tyrosine kinase and growth factor
524 signaling. This group included key regulatory surfaceome molecules such as SMO
525 (smoothened; involved in the Indian Hedgehog (IHH) pathway and hypertrophy (52)), or FZD7
526 (frizzled 7; a Wnt receptor involved in chondroprotection (53)), highlighting the involvement of
527 diverse signaling and adhesion pathways in cartilage biology and prospective OA therapy
528 targets. This cluster contained several proteins without established roles in chondrogenesis,
529 including PODXL (matrix adhesion and phenotype stability) and CNTFR (growth factor
530 signaling and repair).

531 We also performed a detailed PPI network analysis of each surfaceome cluster using
532 STRING (Figure S4). In **Cluster 1**, the PPI network is enriched in ECM remodeling, collagen
533 biosynthesis, and protein folding, with additional roles in vesicle trafficking and oxidative stress
534 response. The PPI network in **Cluster 2** was dominated by ephrin signaling with four Eph
535 receptors, highlighting roles in developmental patterning. Endocytosis and RAB GTPases are
536 central to membrane dynamics and intracellular transport. SRC and FGFR2 link focal

537 adhesion and growth factor signaling. **Cluster 3** is enriched in cytoskeletal organization,
538 calcium signaling, and cell adhesion pathways. Focal adhesion and actin cytoskeleton
539 pathways dominate the network, driven by actinin, myosin, and dystrophin. Calcium signaling
540 may integrate metabolic and inflammatory responses via CALM3 and S100A6. HMGB1 links
541 nuclear DNA repair with extracellular VEGF signaling. **Cluster 4** is dominated by ephrin
542 signaling with several Eph receptors, highlighting roles in cell migration during nodule
543 formation. Wnt and Hedgehog signaling pathways are central to developmental processes.
544 EGFR/FGFRs link growth factor signaling to MAPK activation.
545
546 *5. Surfaceome enrichment enhances detection of low-abundance targets*
547 Comparative analysis revealed limited overlap (23%) between proteins identified in
548 total lysates and surfaceome-enriched fractions (Table S2). Notably, 77% of AOB-enriched
549 proteins were undetectable in total lysates, demonstrating the method's enhanced capacity to
550 resolve low-abundance membrane-associated targets. Conventional whole-cell proteomics is
551 constrained by the dominance of high-abundance cytoplasmic and organellar proteins, which
552 often mask low-abundance surface-residing targets during MS analysis. By selectively
553 enriching surface proteins, our approach mitigates this dynamic range limitation, enabling
554 robust identification of membrane-associated and extracellular proteins that otherwise fall
555 below detection thresholds in unfractionated lysates. This methodological advance
556 underscores the efficacy of this method in resolving biologically critical surfaceome
557 components, which are frequently underrepresented in global proteomic analyses, and
558 highlights its utility for advancing receptor, biomarker, and therapeutic target discovery.
559
560 *6. In silico and in vitro chondrogenic surfaceome*
561 To maximize the identification of cell surface proteins, we inferred cell surface
562 localization for all detected proteins using established GO annotations for cellular component
563 and molecular function (16). We first applied this *in silico* prediction on the total cell lysate

dataset, defining the GO term-based surfaceome of chondrogenic cultures. Of the 5,207 proteins in this dataset, 885 proteins (17%) were predicted to localize to the cell surface.

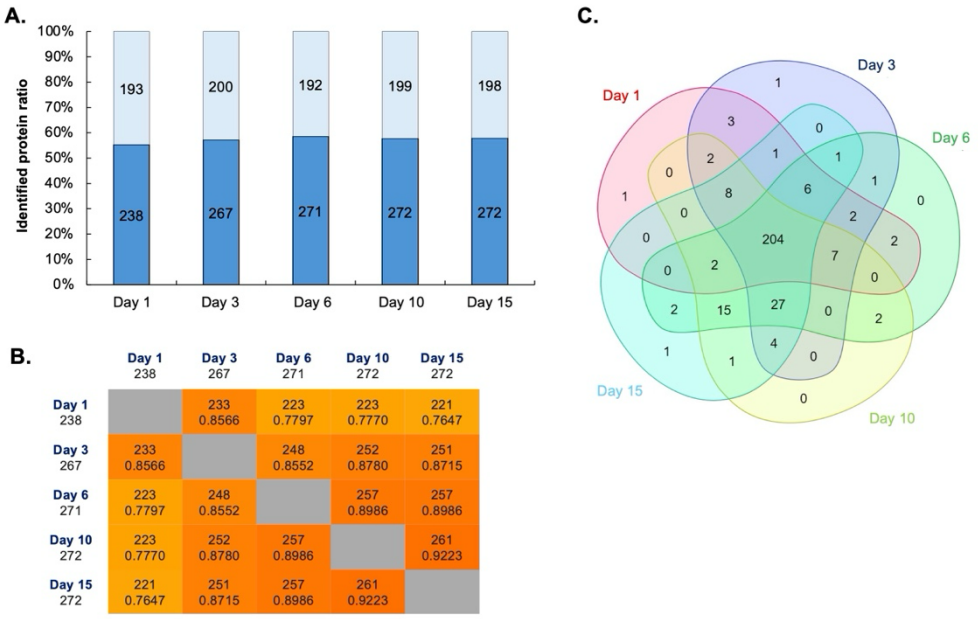

Figure 6. Enrichment of cell surface proteins using the AOB labelling approach. A. Distribution of the 504 surface proteins identified in this study (after manual curation using GO terms; dark bars, core surfaceome; light bars, probably non-surface proteins) between different culture days. **B.** Full symmetrical matrix of the surfaceome proteins across differentiating cultures (integers represent the number of surfaceome proteins; non-integers represent Jaccard indices). **C.** Distribution of the manually curated cell surface proteins identified in this study between micromass cultures of various ages.

We then applied the same approach on the AOB-enriched dataset. The AOB-based enrichment method substantially increased the proportion of identified cell surface proteins, with 55–60% of proteins at all time points and across biological replicates annotated as cell surface-localized (Figure 6A). This represents a significant improvement in the number of surface proteins detected as chondrogenic differentiation progressed, as demonstrated by full symmetrical matrix analysis (Jaccard index) (Figure 6B). We classified the identified surfaceome proteins into major functional categories based on GO molecular function and biological process annotations: enzymes, transporters, receptors, cell junctions and adhesion proteins, ECM components, and unclassified/miscellaneous proteins (including known interacting or binding partners of surface proteins; Table S3). The relative distribution of surface proteins in these categories remained consistent throughout chondrogenesis.

586 We next examined qualitative expression dynamics of the cell surface proteins to
587 identify candidate surface biomarkers specific to the early stages of chondrogenic
588 differentiation (days 1–6). Using Venn diagram analysis of manually curated protein lists
589 across the studied time points (Figure 6C), only two proteins met the criteria for early-stage
590 specificity: ciliary neurotrophic factor receptor (CNTFR) and podocalyxin (PODXL).

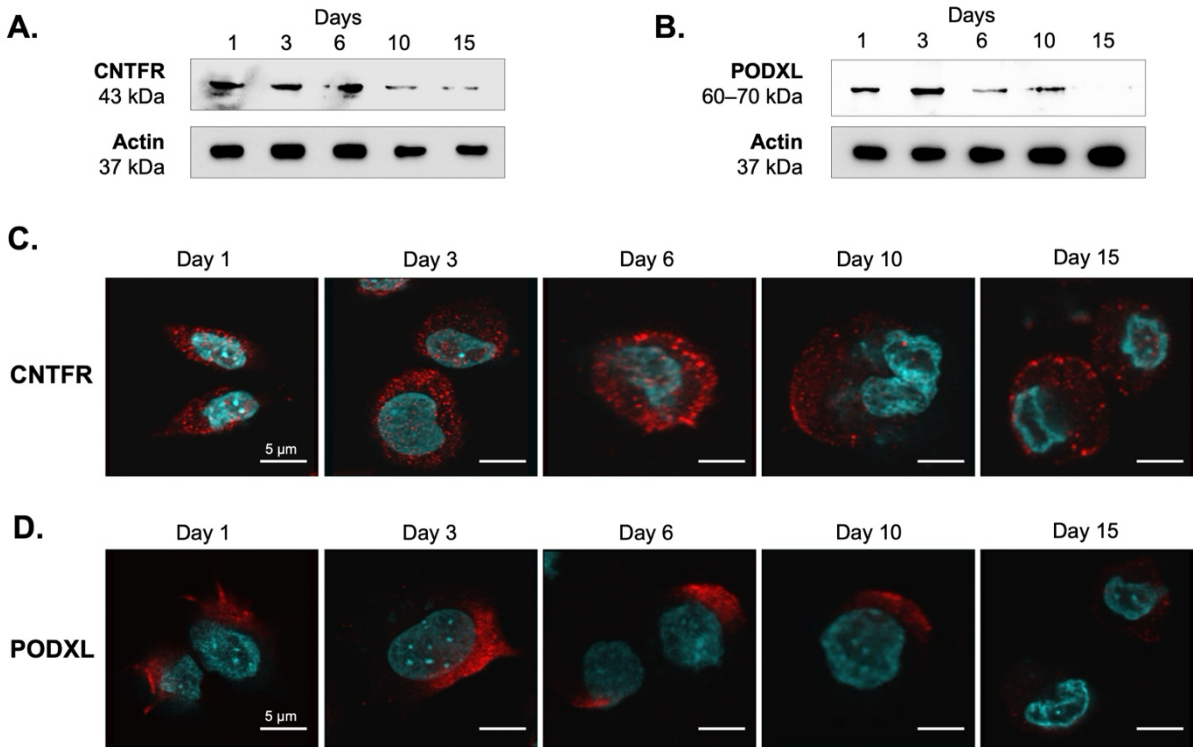

591

592 **Figure 7. Validation of the efficacy and specificity of the AOB-based glycocapture method.**
593 Western blot for CNTFR (**A**) and PODXL (**B**) performed on total cell lysates of micromass cultures.
594 Representative blot image (n = 3). Full-length uncropped blots are presented in Figure S5.
595 Intracellular distribution of CNTFR (**C**) and PODXL (**D**) in cells of micromass cultures detected by
596 immunocytochemistry. Primary antibodies were visualised using Alexa555-conjugated anti-rabbit
597 secondary antibodies (red). Nuclear DNA was stained with DAPI (cyan). Data shown are
598 representative out of 3 independent experiments. Scale bar, 5 µm.

599

600 *7. Validation of CNTFR and PODXL expression*

601 To verify the expression of CNTFR and PODXL during chondrogenesis, we performed
602 western blot analyses on total cell lysates obtained from micromass cultures harvested at the
603 same time points as AOB-enriched samples. Both CNTFR and PODXL were clearly detected
604 on the blots. For CNTFR, a distinct band was observed at approximately 43 kDa, consistent
605 with its predicted molecular mass, and its expression displayed a gradual decrease over the

606 course of differentiation (Figure 7A). Similarly, PODXL was detected as a prominent ~60 kDa
607 band, also showing a progressive downregulation throughout the differentiation period (Figure
608 7B). Notably, the expression patterns of both CNTFR and PODXL closely mirrored the trends
609 observed in our quantitative proteomics analyses performed on the same cultures.

610 To further investigate the subcellular localization of CNTFR and PODXL, we carried
611 out immunocytochemistry followed by confocal microscopy. Both CNTFR and PODXL were
612 localized to the plasma membrane in chondrogenic cells, with additional intracellular staining
613 (Figure 7C–D). Although this analysis was qualitative, both markers appeared to be
614 downregulated at later stages of differentiation, with this trend being particularly pronounced
615 for PODXL. Notably, PODXL was primarily localized at the leading edge of cellular processes,
616 suggesting a potential role in cell morphology or migration during chondrogenesis.

617 To investigate the functional role of CNTFR and PODXL in our chondrogenic model,
618 we analyzed their regulatory networks using transcriptomic and proteomic data. STRING-
619 derived interaction network for both proteins (top 25 interactants) were cross-referenced with
620 expression profiles from our previously published RNA-seq dataset (17) of the same
621 chondrogenic model, and total lysate proteomics.

622 For CNTFR, 21 of the 25 interactants were expressed at the transcript level (Figures
623 S6–S7), and 8 also detected as proteins in the total lysates. PODXL showed expression of 14
624 interactant transcripts and 8 corresponding proteins. Weighted gene co-expression network
625 analysis (WGCNA) of RNA-seq data, using CNTFR or PODXL expression levels across
626 different samples as a trait, revealed clusters of genes highly correlated with CNTFR or
627 PODXL expression. Therefore, we screened the proximal associated proteins of CNTFR or
628 PODXL and their top 25 interactants within significantly correlated modules and integrated
629 them. The rationale behind this approach was to check the enrichment of GO information in
630 the co-expression modules. For CNTFR, five module eigengenes (MEs) were showing
631 significant degree of correlation (with the turquoise module showing the strongest correlation
632 to the trait), indicating that genes in these MEs may be associated with CNTFR or its top 25
633 interactants. We therefore performed functional enrichment analysis on these modules, in

634 which GO terms related to tyrosine phosphorylation, cell adhesion, cytokine and growth factor
635 activity, PI3K/Akt and MAPK pathways were enriched. For PODXL, out of five MEs showing
636 high degree of correlation with the gene and its interactants, the black ME displayed the
637 strongest correlation to the trait, in which GO terms such as cell-cell junction, potassium
638 channel activity, differentiation and morphogenesis were over-represented.

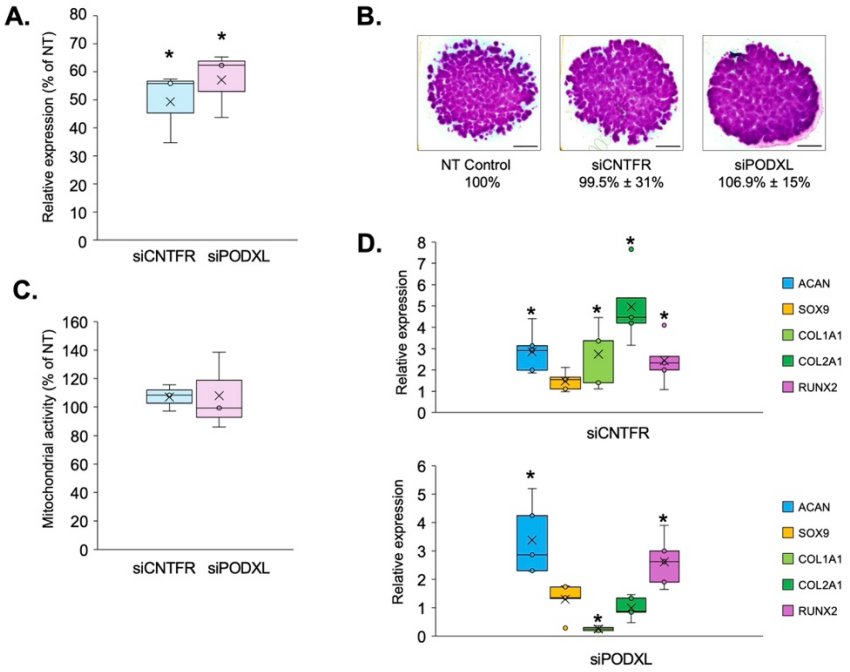

639

640 **Figure 8. Effects of transient gene silencing of CNTFR or PODXL on osteochondral marker**
641 **gene expression profiles and cartilage matrix production. A.** Quantitative RT-qPCR analysis of
642 CNTFR and PODXL mRNA levels in micromass cultures 48 hours post-transfection with
643 target-specific siRNAs. Expression values are shown as fold change relative to non-targeting (NT)
644 control, normalized to the reference gene *RPS7*. Data represent mean ± SEM (n = 3). Asterisks
645 indicate significant differences relative to NT controls ($p < 0.05$). **B.** Representative DMMB-stained
646 micromass cultures at day 6 illustrating cartilage matrix deposition after transient CNTFR or PODXL
647 silencing compared with NT control. Scale bar = 1 mm. The lower panel shows the corresponding
648 MATLAB-based quantitative analysis of metachromatic area normalized to NT = 100%. Data are
649 mean ± SEM (n = 3). **C.** MTT assay results reflecting relative cell viability in day 6 cultures after
650 silencing. Values are expressed as percentage of NT control (mean ± SEM, n = 3). **D.** Expression of
651 key osteochondrogenic marker genes (*COL1A1, COL2A1, ACAN, RUNX2*) examined 48 hours after
652 transfection. Values represent fold change versus NT control, normalized to *RPS7*. Data are mean ±
653 SEM (n = 3); asterisks indicate $p < 0.05$.
654

655 *8. Transient gene silencing of CNTFR and PODXL*

656 To evaluate the functional impact of CNTFR and PODXL on matrix gene regulation,
657 we performed transient siRNA-mediated silencing in primary chondrogenic progenitor cells
658 prior to seeding as micromass cultures (culture day 0). Transfection efficiency and gene

659 silencing were confirmed in 2-day-old cultures (48 hours post-transfection), with *CNTFR* and
660 *PODXL* transcript levels reduced by approximately 57% and 49%, respectively, relative to the
661 non-targeting (NT) control (Figure 8A).

662 Although the DMMB-stained micromass cultures (Figure 8B) did not exhibit overt
663 qualitative differences in metachromatic intensity across experimental groups, we additionally
664 performed quantitative image analysis to ensure objective comparison of matrix yield. Using
665 MATLAB-based area quantification normalized to the non-targeting (NT) control (set
666 as 100%), the mean ± SEM values confirmed that total metachromatic matrix deposition
667 remained statistically unchanged following transient knockdown of *CNTFR* or *PODXL* (n = 3).
668 This finding supports the notion that the limited 48-hour window after siRNA treatment is
669 sufficient to capture early transcriptional but not morphological effects, as ECM accumulation
670 in this model typically becomes detectable only several days later. Similarly, cell viability and
671 proliferation remained unaffected on day 6 as assessed by MTT assay (Figure 8C).

672 However, RT-qPCR analysis performed 48 hours post-transfection revealed distinct
673 transcriptional effects on osteochondrogenic marker gene expression, consistent with early
674 transcriptional rather than morphological responses (Figure 8D). *CNTFR* silencing resulted in
675 marked upregulation of *ACAN* (2.9-fold), *COL2A1* (4.9-fold), *RUNX2* (2.5-fold), and *COL1A1*
676 (2.7-fold) relative to non-targeting (NT) control cultures, whereas *PODXL* silencing increased
677 *ACAN* (3.3-fold) and *RUNX2* (2.6-fold) expression but downregulated *COL1A1* (–3.8-fold).
678 These divergent transcriptional responses indicate that *CNTFR* and *PODXL* differentially
679 modulate ECM-related gene networks, potentially influencing the matrix composition rather
680 than its total production.

681 Although neither perturbation affected observable changes in ECM deposition or
682 proliferation, these findings highlight distinct effects on transcriptional regulation of ECM-
683 associated genes by *CNTFR* and *PODXL*. The contrasting modulation of *COL1A1* suggests
684 that these surface proteins may influence the qualitative composition and molecular specificity
685 of the ECM during chondrogenesis. Furthermore, the observed expression patterns reinforce

686 the concept that *PODXL* and *CNTFR* act as early regulatory nodes, modulating transcriptional

687 programs that precede measurable ECM remodeling during chondrogenesis.

688

689 **Discussion**

690 In this work, we identify podocalyxin (PODXL) and ciliary neurotrophic factor receptor
691 (CNTFR) as previously unrecognized cell surface constituents of chondrogenic progenitor
692 cells. By employing a glycocapture-assisted subproteome enrichment strategy combined with
693 high-throughput shotgun mass spectrometry, we achieved enhanced sensitivity for detecting
694 low-abundance surface compared to conventional whole-cell and surfaceome profiling
695 proteomics approaches, as demonstrated in earlier studies (10, 16, 54). While similar
696 enrichment and mass spectrometry-based workflows have previously been applied to
697 characterize the surfaceome of mesenchymal cells and primary equine chondrocytes under
698 normal and pro-inflammatory conditions (9, 15), the present work complements and extends
699 this methodology to systematically and quantitatively profile dynamic changes in the
700 surfaceome during *in vitro* chondrogenic differentiation in embryonic progenitor cells. Our
701 study offers a temporal and functional proteomic map of the chondrogenic cell surface in a
702 developmental (non-inflammatory) context, widening the molecular framework for
703 understanding how membrane proteins contribute to cartilage lineage specification and
704 phenotype stability.

705

706 *CNTFR and implications for chondrogenesis*

707 The identification of CNTFR in differentiating chondrocytes opens new perspectives
708 on neurotrophic cytokine signaling in cartilage biology. Ciliary neurotrophic factor (CNTF), a
709 member of the interleukin-6 (IL-6) family, signals through a tripartite receptor complex
710 comprising CNTFRα, gp130, and LIFR (55, 56). Initially characterized as a neuronal survival
711 and differentiation factor, CNTF has since been implicated in multiple tissues, including bone
712 and cartilage (57-59). Related ligands such as cardiotrophin-like cytokine (CLCF1) also
713 influence MSC differentiation and osteogenesis (60), reinforcing the idea of a functional role
714 for CNTF/CNTFR signaling in skeletal development (61).

715 CNTFR expression has known roles in cartilage homeostasis and OA progression. For
716 instance, upregulation of the CRLF1/CLCF1 complex, which competes with CNTF for CNTFR

717 binding, disrupts cartilage ECM homeostasis and exacerbates OA (58). Our finding of
718 persistent CNTFR expression during chondrogenesis, coupled with its plasma membrane
719 localization in differentiating chondrocytes, suggests dual roles in cartilage maintenance and
720 pathological remodeling. This positions CNTFR as both a mechanistic regulator and potential
721 therapeutic target in OA.

722 Our observation aligns with previous findings on signaling-driven regulation of
723 chondrogenic differentiation. In particular, comprehensive analyses of cartilage lineage
724 specification (62) and recent single-cell and transcriptomic profiling of chondrocyte
725 subpopulations (8) highlighted the interplay between growth factor–mediated pathways
726 (including IL-6 family cytokines, FGFR, and TGF-β signaling) and ECM remodeling as key
727 determinants of progenitor maintenance and hypertrophic transition. Our results suggest that
728 CNTFR activity may function within this network, modulating survival and fibrocartilaginous
729 remodeling responses during differentiation.

730

731 *Podocalyxin and progenitor state regulation*

732 Podocalyxin (PODXL), classically associated with kidney podocytes and vascular
733 endothelium, is a member of the CD34 transmembrane sialomucin family (63). It contributes
734 to cell adhesion, migration, and progenitor cell maintenance (64, 65). Its presence in
735 chondrogenic cells is novel and suggests potential roles in modulating progenitor cell
736 responses to chondrogenic cues such as SOX9 and TGF-β signaling (66). This is conceptually
737 consistent with previous studies demonstrating dynamic modulation of cell-matrix receptors
738 and cytoskeletal regulators during the dedifferentiation-redifferentiation cycle of chondrocytes
739 (62). Moreover, at the single-cell level, progenitor-like clusters characterized by strong
740 expression of adhesion and polarity molecules were described (8), a feature reminiscent of
741 PODXL-positive states in our study. Together, these findings support the hypothesis that
742 PODXL may contribute to the maintenance of a transitional chondrogenic phenotype with
743 migratory or matrix-adaptation potential. While evidence directly linking PODXL to

744 chondrogenesis is limited, its downregulation during osteogenic maturation and association
745 with progenitor-rich MSC populations highlight it as a candidate regulator of early cartilage
746 differentiation.
747
748 *Opposing roles in ECM quality control*
749 Our transient knockdown assays revealed opposing transcriptional regulation of
750 *COL1A1*, a well-known marker of fibrocartilage and mechanically compromised repair tissue
751 (62, 67), by *PODXL* and *CNTFR*. *CNTFR* silencing increased *COL1A1* expression (2.7-fold),
752 whereas *PODXL* silencing reduced it (−3.8-fold). The differential regulation of *COL1A1*
753 between the two knockdowns suggests that these proteins influence ECM-related
754 transcription through distinct pathways. PODXL may help sustain fibrogenic signaling (via β1-
755 integrin/FAK pathways) (68, 69), while CNTFR loss may mimic cytokine deprivation stress,
756 and trigger compensatory fibrotic responses, possibly through ERK/STAT3 signaling cross-
757 talk, reminiscent of synovial fibrosis in OA via impaired signaling (70). Thus, the responses
758 observed here are consistent with the predicted biological roles of CNTFR and PODXL, which
759 are reflected in the network associations shown in Figure S7.
760 The absence of overt changes in ECM production in our knockdown model suggests
761 functional redundancy in matrix remodeling, post-transcriptional regulation, or compensation
762 by other surface receptors. Quantitative evaluation of DMMB-positive areas using
763 MATLAB-based image analysis further confirmed that total matrix deposition was not
764 significantly altered by either treatment. The absence of visible or quantitative differences
765 therefore likely reflects the temporal separation between transcriptional and phenotypic
766 responses, rather than true lack of functional relevance.
767
768 *Translational implications*
769 Single-cell RNA-seq analysis of human articular chondrocytes revealed detectable
770 transcripts for both *CNTFR* (predominantly in effector and homeostatic chondrocytes) and
771 *PODXL* (at lower levels in *VEGFA*$^{+}$ cells, fibrochondrocytes, and pre-hypertrophic

772 chondrocytes) (Figure S8). This, combined with their extracellular accessibility, positions
773 CNTFR and PODXL as potentially detectable biomarkers in synovial fluid or serum, opening
774 avenues for early OA diagnosis and therapeutic monitoring.

775 Beyond their diagnostic potential, modulating PODXL-mediated cell-matrix
776 interactions or CNTFR-dependent signaling could open new, targeted approaches to cartilage
777 repair or OA management (71). While functional redundancy in chondrogenic signaling
778 networks or compensatory mechanisms from other surface receptors may mask direct
779 phenotypic impact in single knockdowns, combinatorial gene perturbations or pathway-
780 focused interventions could reveal their full regulatory capacity.

781

782 *Limitations*

783 The use of chicken embryonic limb bud-derived chondrogenic progenitor cells provides
784 a valuable developmental model but may not fully recapitulate all aspects of human
785 chondrogenesis or OA pathophysiology. While the embryonic avian limb model has been
786 extensively validated as a mechanistic system for studying cartilage differentiation, species-
787 specific variations in ECM composition, signaling dynamics, and progenitor populations may
788 limit the direct extrapolation of our findings to human articular cartilage. Similarly, the
789 micromass culture system, although well-established for modeling chondrogenic lineage
790 commitment (18), remains a simplified *in vitro* system that cannot reproduce the full cellular
791 complexity, mechanical stimuli, or biochemical heterogeneity present in the native joint
792 environment.

793 Our cell surface protein enrichment workflow focused on N-linked glycosylated plasma
794 membrane constituents, which ensures strong selectivity for *bona fide* surface proteins but
795 may underrepresent other biologically important groups such as non-glycosylated or O-linked
796 membrane proteins and secreted matrix components. Consequently, certain signaling or
797 adhesion receptor families involved in chondrogenic regulation may not have been captured.
798 In addition, although Gene Ontology (GO) annotation was performed using human ortholog

799 mapping to facilitate cross-species interpretation, specific biological processes may be unique
800 to avian systems or not entirely conserved between chicken and human cartilage (72, 73).
801 In addition, functional redundancy among surface receptors may partially mask
802 morphological or matrix-level phenotypes, as parallel signaling pathways can compensate for
803 transient loss of individual components. The transient siRNA-based functional assays for
804 *PODXL* and *CNTFR* were intentionally designed to capture short-term transcriptional
805 responses; however, such brief modulation may not fully reveal cumulative effects on
806 long-term ECM assembly, organization, or mechanical integrity.
807 Future studies incorporating human chondrogenic progenitors or patient-derived
808 chondrocyte models, coupled with more comprehensive surfaceome coverage and stable
809 gene perturbation strategies, will be necessary to confirm the translational relevance and fully
810 delineate the downstream signaling networks of these proteins and confirm the translational
811 relevance of the observed regulatory patterns. Fully comprehensive surfaceome profiling of
812 chondrogenic and mature chondrocytes will ultimately require integration of alternative
813 enrichment chemistries, spatial proteomics, and cell types, as well as deeper sampling under
814 both physiological and disease-mimicking conditions.
815

816 **Conclusions**

817 In summary, we map the dynamic surfaceome of chondrogenic cells and identify
818 PODXL and CNTFR as newly identified components at the interface of cell communication,
819 adhesion, and survival signaling, showing expression dynamics consistent with roles in ECM
820 regulation. These findings deepen our understanding of chondrocyte surface signaling
821 networks, hold promise for biomarker development and could inform therapeutic strategies in
822 OA and cartilage regeneration.

823 Our study contributes new insight into surfaceome remodeling during embryonic
824 chondrogenesis. The candidate surface proteins identified here provide a basis for further
825 discovery efforts and functional exploration under a wider range of conditions. Future studies
826 in human cellular and disease models will be crucial to determine their diagnostic and
827 therapeutic potential. Furthermore, follow-up studies will be needed to expand the surfaceome
828 landscape under diverse physiological (e.g., hormonally regulated, loaded cartilage) and
829 pathological (inflammatory, OA-like) conditions. The dynamic and context-dependent nature
830 of the chondrocyte surfaceome warrants integration of multiple complementary strategies,
831 including alternative cell models, stimuli, and orthogonal enrichment techniques to approach
832 a more complete characterization.

833

834 **Additional files (Supplementary material)**

835

836 - Additional file 1 (PDF) contains Supplementary Figures S1–S8 and Supplementary
837 Tables S1–S3, providing additional data supporting the main findings.
838 - Additional files 2–5 (Excel spreadsheets) include: differential expression analysis and
839 clustering results for total lysate proteomes (files 2–3) and surfaceome proteomes (files
840 4–5). Collectively, these materials offer expanded experimental details, data
841 visualizations, and full quantitative proteomic datasets underlying the study.

842

843

844 **DECLARATIONS**

845 **Ethics approval and consent to participate**

846 Not applicable to thus manuscript.

847

848 **Consent for publication**

849 Not applicable to thus manuscript.

850

851 **Availability of data and materials**

852 The dataset supporting the conclusions of this article is available in the ProteomeXchange
853 Consortium *via* the PRIDE partner repository with the dataset identifier PXD064013
854 (https://www.ebi.ac.uk/pride/archive/projects/PXD064013/private)

855

856 **Competing interests**

857 The authors declare that they have no conflicts of interest. The authors wrote this paper within
858 the scope of their academic and research positions. None of the authors has any relationships
859 that could be construed as biased or inappropriate. Funding bodies were not involved in the
860 study design, data collection, analysis, or interpretation. The decision to submit this paper for
861 publication was not influenced by any funding bodies.

Funding

This paper was supported by the János Bolyai Research Scholarship of the Hungarian Academy of Sciences, awarded to CM. CM was supported by the Young Researcher Excellence Programme (grant number: FK-134304) of the National Research, Development and Innovation Office, Hungary. This research was supported by the EKÖP-24-4 and EKÖP-24-3 University Research Fellowship Programme of the Ministry for Culture and Innovation from the source of the National Research, Development and Innovation Fund, Hungary, awarded to RT (EKÖP-24-4-II-DE-58), KJ (EKÖP-24-3-I-DE-290) and PK (EKÖP-24-3-II-DE-1). PK was supported by the PhD Excellence Scholarship from the Count István Tisza Foundation for the University of Debrecen. CM and RT also acknowledge financial support from the European Cooperation in Science and Technology COST Association Action CA21110 - Building an open European Network on OsteoArthritis research (NetwOArk); https://www.cost.eu/actions/CA21110/). This research was supported by the University of Debrecen Program for Scientific Publication, and by the National Academy of Scientist Education Program in Hungary.

Authors' contributions

All authors made substantial contributions to discussion of the content, writing of the original outline, and reviewing/editing of the article before submission. All authors approve the final version for publication and agree to be accountable for the accuracy and integrity of the study. Patrik Kovács: Formal analysis, Methodology, Validation, Visualisation, Writing—original draft, Writing—review & editing. Peter Brazda: Formal analysis, Visualisation, Writing—original draft, Writing—review & editing. Tibor Hajdú: Formal analysis, Methodology, Writing—original draft, Writing—review & editing. Boglárka Harsányi: Formal analysis, Methodology, Writing—original draft. Krisztián Juhász: Formal analysis, Methodology, Writing—original draft. Roland Takács: Formal analysis, Methodology, Validation, Writing—original draft, Writing—review & editing. Judit Vágó: Formal analysis, Methodology, Writing—original draft, Writing—review &

editing. Zhangzgeng Wang: Formal analysis, Methodology, Writing—original draft, Writing—review & editing. Clare Coveney: Formal analysis, Methodology, Writing—original draft, Writing—review & editing. David J. Boocock: Formal analysis, Software, Methodology, Visualization, Writing—original draft, Writing—review & editing. Csaba Matta: Conceptualization, Formal analysis, Funding acquisition, Methodology, Supervision, Validation, Writing—original draft, Writing—review & editing.

Acknowledgements

The authors thank Mrs. Krisztina Bíróné Barna and Ms. Éva Katona from the Department of Anatomy, Histology and Embryology, and Prof. Éva Csősz and Mrs. Julianna Kökényesiné Csáki from the Proteomics Core Facility, Department of Biochemistry and Molecular Biology, Faculty of Medicine, University of Debrecen, for technical assistance.

References

1. Mobasheri A, Thudium CS, Bay-Jensen AC, Maleitzke T, Geissler S, Duda GN, et al. Biomarkers for osteoarthritis: Current status and future prospects. Best Pract Res Clin Rheumatol. 2023;37(2):101852.
2. Tong L, Yu H, Huang X, Shen J, Xiao G, Chen L, et al. Current understanding of osteoarthritis pathogenesis and relevant new approaches. Bone Res. 2022;10(1):60.
3. Rodriguez-Merchan EC. The Current Role of Disease-modifying Osteoarthritis Drugs. Arch Bone Jt Surg. 2023;11(1):11-22.
4. Maqbool M, Fekadu G, Jiang X, Bekele F, Tolossa T, Turi E, et al. An up to date on clinical prospects and management of osteoarthritis. Ann Med Surg (Lond). 2021;72:103077.
5. Richardson SM, Kalamegam G, Pushparaj PN, Matta C, Memic A, Khademhosseini A, et al. Mesenchymal stem cells in regenerative medicine: Focus on articular cartilage and intervertebral disc regeneration. Methods. 2016;99:69-80.
6. Muthu S, Korpershoek JV, Novais EJ, Tawy GF, Hollander AP, Martin I. Failure of cartilage regeneration: emerging hypotheses and related therapeutic strategies. Nat Rev Rheumatol. 2023;19(7):403-16.
7. Im GI, Kim TK. Regenerative Therapy for Osteoarthritis: A Perspective. Int J Stem Cells. 2020;13(2):177-81.
8. Matta C, Takacs R, Dvir-Ginzberg M, Richardson SM, Pelttari K, Pattappa G, et al. Insights into chondrocyte populations in cartilaginous tissues at the single-cell level. Nat Rev Rheumatol. 2025;21(8):465-77.
9. Matta C, Boocock DJ, Fellows CR, Miosge N, Dixon JE, Liddell S, et al. Molecular phenotyping of the surfaceome of migratory chondroprogenitors and mesenchymal stem cells using biotinylation, glycocapture and quantitative LC-MS/MS proteomic analysis. Sci Rep. 2019;9(1):9018.
10. Pauwels J, Fijalkowska D, Eyckerman S, Gevaert K. Mass spectrometry and the cellular surfaceome. Mass Spectrom Rev. 2022;41(5):804-41.

11. Takacs R, Mobasheri A, Matta C. Introduction: Methods for Studying the Plasma Membrane and the Surfaceome. Methods Mol Biol. 2025;2908:1-9.
12. Alegre-Aguaron E, Desportes P, Garcia-Alvarez F, Castiella T, Larrad L, Martinez-Lorenzo MJ. Differences in surface marker expression and chondrogenic potential among various tissue-derived mesenchymal cells from elderly patients with osteoarthritis. Cells Tissues Organs. 2012;196(3):231-40.
13. Lu Z, Yan L, Pei M. Commentary on 'Surface markers associated with chondrogenic potential of human mesenchymal stromal/stem cells'. F1000Res. 2020;9.
14. Kalamegam G, Memic A, Budd E, Abbas M, Mobasheri A. A Comprehensive Review of Stem Cells for Cartilage Regeneration in Osteoarthritis. Adv Exp Med Biol. 2018;1089:23-36.
15. Jeremiasse B, Matta C, Fellows CR, Boocock DJ, Smith JR, Liddell S, et al. Alterations in the chondrocyte surfaceome in response to pro-inflammatory cytokines. BMC Mol Cell Biol. 2020;21(1):47.
16. Kovacs P, Boocock DJ, Coveney C, Mobasheri A, Matta C. Aminooxy Biotin-Based Characterization of the Surfaceome of Chondrogenic Cells. Methods Mol Biol. 2025;2908:65-79.
17. Takacs R, Vago J, Poliska S, Pushparaj PN, Ducza L, Kovacs P, et al. The temporal transcriptomic signature of cartilage formation. Nucleic Acids Res. 2023;51(8):3590-617.
18. Takacs R, Juhasz T, Katona E, Somogyi C, Vago J, Hajdu T, et al. Isolation and Micromass Culturing of Primary Chicken Chondroprogenitor Cells for Cartilage Regeneration. Curr Protoc. 2023;3(7):e835.
19. Demichev V, Messner CB, Vernardis SI, Lilley KS, Ralser M. DIA-NN: neural networks and interference correction enable deep proteome coverage in high throughput. Nat Methods. 2020;17(1):41-4.
20. Ranathunge C, Patel SS, Pinky L, Correll VL, Chen S, Semmes OJ, et al. promor: a comprehensive R package for label-free proteomics data analysis and predictive modeling. Bioinform Adv. 2023;3(1):vbad025.
21. Matta C, Juhasz T, Fodor J, Hajdu T, Katona E, Szucs-Somogyi C, et al. N-methyl-D-aspartate (NMDA) receptor expression and function is required for early chondrogenesis. Cell Commun Signal. 2019;17(1):166.
22. Pfaffl MW, Tichopad A, Prgomet C, Neuvians TP. Determination of stable housekeeping genes, differentially regulated target genes and sample integrity: BestKeeper--Excel-based tool using pair-wise correlations. Biotechnol Lett. 2004;26(6):509-15.
23. Kita K, Kimura T, Nakamura N, Yoshikawa H, Nakano T. PI3K/Akt signaling as a key regulatory pathway for chondrocyte terminal differentiation. Genes Cells. 2008;13(8):839-50.
24. Zhang H, Chen X, Xue P, Ma X, Li J, Zhang J. FN1 promotes chondrocyte differentiation and collagen production via TGF-beta/PI3K/Akt pathway in mice with femoral fracture. Gene. 2021;769:145253.
25. Liu CF, Lefebvre V. The transcription factors SOX9 and SOX5/SOX6 cooperate genome-wide through super-enhancers to drive chondrogenesis. Nucleic Acids Res. 2015;43(17):8183-203.
26. Haller R, Schwanbeck R, Martini S, Bernoth K, Kramer J, Just U, et al. Notch1 signaling regulates chondrogenic lineage determination through Sox9 activation. Cell Death Differ. 2012;19(3):461-9.
27. Fukumoto T, Sanyal A, Fitzsimmons JS, O'Driscoll SW. Expression of beta1 integrins during periosteal chondrogenesis. Osteoarthritis Cartilage. 2002;10(2):135-44.
28. Yagi H, Takahata Y, Murakami T, Nakaminami Y, Hagino H, Yamamoto S, et al. Transcriptional regulation of FRZB in chondrocytes by Osterix and Msx2. J Bone Miner Metab. 2022;40(5):723-34.
29. Wang W, Rigueur D, Lyons KM. TGFbeta signaling in cartilage development and maintenance. Birth Defects Res C Embryo Today. 2014;102(1):37-51.
30. Zhang F, Wang Y, Zhao Y, Wang M, Zhou B, Zhou B, et al. NFATc1 marks articular cartilage progenitors and negatively determines articular chondrocyte differentiation. Elife. 2023;12.
31. Niu J, Liu Y, Wang J, Wang H, Zhao Y, Zhang M. Thrombospondin-2 acts as a critical regulator of cartilage regeneration: A review. Medicine (Baltimore). 2023;102(17):e33651.

32. Wang Y, Wen X, Guo Y, Wang Y, Gu Y. TFRC Ablation Induces Insufficient Cartilage Development Through Mitochondrial p53 Translocation-Mediated Ferroptosis. Int J Mol Sci. 2025;26(6).
33. Rigueur D, Brugger S, Anbarchian T, Kim JK, Lee Y, Lyons KM. The type I BMP receptor ACVR1/ALK2 is required for chondrogenesis during development. J Bone Miner Res. 2015;30(4):733-41.
34. Li Q, Han B, Wang C, Tong W, Wei Y, Tseng WJ, et al. Mediation of Cartilage Matrix Degeneration and Fibrillation by Decorin in Post-traumatic Osteoarthritis. Arthritis Rheumatol. 2020;72(8):1266-77.
35. Salminen-Mankonen H, Saamanen AM, Jalkanen M, Vuorio E, Pirila L. Syndecan-1 expression is upregulated in degenerating articular cartilage in a transgenic mouse model for osteoarthritis. Scand J Rheumatol. 2005;34(6):469-74.
36. Gruber BL, Mienaltowski MJ, MacLeod JN, Schittny J, Kasper S, Fluck M. Tenascin-C expression controls the maturation of articular cartilage in mice. BMC Res Notes. 2020;13(1):78.
37. Michelacci YM, Baccarin RYA, Rodrigues NNP. Chondrocyte Homeostasis and Differentiation: Transcriptional Control and Signaling in Healthy and Osteoarthritic Conditions. Life (Basel). 2023;13(7).
38. Choocheep K, Hatano S, Takagi H, Watanabe H, Kimata K, Kongtawelert P, et al. Versican facilitates chondrocyte differentiation and regulates joint morphogenesis. J Biol Chem. 2010;285(27):21114-25.
39. Huang J, Huang J, Li N, Wang L, Xiao Q. FBN2 promotes the proliferation, mineralization, and differentiation of osteoblasts to accelerate fracture healing. Sci Rep. 2025;15(1):4843.
40. Bartoletti G, Dong C, Umar M, He F. Pdgfra regulates multipotent cell differentiation towards chondrocytes via inhibiting Wnt9a/beta-catenin pathway during chondrocranial cartilage development. Dev Biol. 2020;466(1-2):36-46.
41. Ishida O, Tanaka Y, Morimoto I, Takigawa M, Eto S. Chondrocytes are regulated by cellular adhesion through CD44 and hyaluronic acid pathway. J Bone Miner Res. 1997;12(10):1657-63.
42. Oldefest M, Dusterhoft S, Desel C, Thysen S, Fink C, Rabe B, et al. Secreted Frizzled-related protein 3 (sFRP3)-mediated suppression of interleukin-6 receptor release by A disintegrin and metalloprotease 17 (ADAM17) is abrogated in the osteoarthritis-associated rare double variant of sFRP3. Biochem J. 2015;468(3):507-18.
43. O'Conor CJ, Leddy HA, Benefield HC, Liedtke WB, Guilak F. TRPV4-mediated mechanotransduction regulates the metabolic response of chondrocytes to dynamic loading. Proc Natl Acad Sci U S A. 2014;111(4):1316-21.
44. Zhang J, Zhang S, Zhou Y, Qu Y, Hou T, Ge W, et al. KLF9 and EPYC acting as feature genes for osteoarthritis and their association with immune infiltration. J Orthop Surg Res. 2022;17(1):365.
45. Kimura T, Okada A, Yatabe T, Okubo M, Toyama Y, Noda M, et al. RECK is up-regulated and involved in chondrocyte cloning in human osteoarthritic cartilage. Am J Pathol. 2010;176(6):2858-67.
46. Hellingman CA, Koevoet W, Kops N, Farrell E, Jahr H, Liu W, et al. Fibroblast growth factor receptors in in vitro and in vivo chondrogenesis: relating tissue engineering using adult mesenchymal stem cells to embryonic development. Tissue Eng Part A. 2010;16(2):545-56.
47. Arthur A, Gronthos S. Eph-Ephrin Signaling Mediates Cross-Talk Within the Bone Microenvironment. Front Cell Dev Biol. 2021;9:598612.
48. Bursell L, Woods A, James CG, Pala D, Leask A, Beier F. Src kinase inhibition promotes the chondrocyte phenotype. Arthritis Res Ther. 2007;9(5):R105.
49. Pan J, Ho M. Role of glypican-1 in regulating multiple cellular signaling pathways. Am J Physiol Cell Physiol. 2021;321(5):C846-C58.
50. Wen X, Li X, Tang Y, Tang J, Zhou S, Xie Y, et al. Chondrocyte FGFR3 Regulates Bone Mass by Inhibiting Osteogenesis. J Biol Chem. 2016;291(48):24912-21.
51. Yang L, Gong K, Ren G, Chen B. The Annexin A1 Protein Mimetic Peptide Ac2-26 prevents cellular senescence of CHON-001 chondrocytes against tumor necrosis factor-alpha via the Nrf2/NF-kappaB pathway. Biotechnol Appl Biochem. 2025;72(3):755-65.

1043 52. Luan J, Tao H, Su Y. Taladegib controls early chondrocyte hypertrophy via inhibiting
1044 smoothened/Gli1 pathway. Am J Transl Res. 2020;12(5):1985-93.
1045 53. Ding Z, Lu W, Dai C, Huang W, Liu F, Shan W, et al. The CRD of Frizzled 7 exhibits
1046 chondroprotective effects in osteoarthritis via inhibition of the canonical Wnt3a/beta-catenin
1047 signaling pathway. Int Immunopharmacol. 2020;82:106367.
1048 54. Lee MC, Sun B. Glycopeptide capture for cell surface proteomics. J Vis Exp. 2014(87).
1049 55. Pasquin S, Sharma M, Gauchat JF. Ciliary neurotrophic factor (CNTF): New facets of an old
1050 molecule for treating neurodegenerative and metabolic syndrome pathologies. Cytokine
1051 Growth Factor Rev. 2015;26(5):507-15.
1052 56. Sleeman MW, Anderson KD, Lambert PD, Yancopoulos GD, Wiegand SJ. The ciliary
1053 neurotrophic factor and its receptor, CNTFR alpha. Pharm Acta Helv. 2000;74(2-3):265-72.
1054 57. Askmyr M, White KE, Jovic T, King HA, Quach JM, Maluenda AC, et al. Ciliary neurotrophic
1055 factor has intrinsic and extrinsic roles in regulating B cell differentiation and bone structure.
1056 Sci Rep. 2015;5:15529.
1057 58. Crisponi L, Buers I, Rutsch F. CRLF1 and CLCF1 in Development, Health and Disease. Int J
1058 Mol Sci. 2022;23(2).
1059 59. McGregor NE, Poulton IJ, Walker EC, Pompolo S, Quinn JM, Martin TJ, et al. Ciliary
1060 neurotrophic factor inhibits bone formation and plays a sex-specific role in bone growth and
1061 remodeling. Calcif Tissue Int. 2010;86(3):261-70.
1062 60. Nahle S, Pasquin S, Laplante V, Rousseau F, Sharma M, Gauchat JF. Cardiotrophin-like
1063 cytokine (CLCF1) modulates mesenchymal stem cell osteoblastic differentiation. J Biol
1064 Chem. 2019;294(32):11952-9.
1065 61. Tsuritani K, Takeda J, Sakagami J, Ishii A, Eriksson T, Hara T, et al. Cytokine receptor-like
1066 factor 1 is highly expressed in damaged human knee osteoarthritic cartilage and involved in
1067 osteoarthritis downstream of TGF-beta. Calcif Tissue Int. 2010;86(1):47-57.
1068 62. Dehne T, Schenk R, Perka C, Morawietz L, Pruss A, Sittinger M, et al. Gene expression
1069 profiling of primary human articular chondrocytes in high-density micromasses reveals
1070 patterns of recovery, maintenance, re- and dedifferentiation. Gene. 2010;462(1-2):8-17.
1071 63. Le Tran N, Wang Y, Nie G. Podocalyxin in Normal Tissue and Epithelial Cancer. Cancers
1072 (Basel). 2021;13(12).
1073 64. Larrucea S, Butta N, Arias-Salgado EG, Alonso-Martin S, Ayuso MS, Parrilla R. Expression
1074 of podocalyxin enhances the adherence, migration, and intercellular communication of cells.
1075 Exp Cell Res. 2008;314(10):2004-15.
1076 65. Lee RH, Seo MJ, Pulin AA, Gregory CA, Ylostalo J, Prockop DJ. The CD34-like protein
1077 PODXL and alpha6-integrin (CD49f) identify early progenitor MSCs with increased
1078 clonogenicity and migration to infarcted heart in mice. Blood. 2009;113(4):816-26.
1079 66. Chen H, Tan XN, Hu S, Liu RQ, Peng LH, Li YM, et al. Molecular Mechanisms of
1080 Chondrocyte Proliferation and Differentiation. Front Cell Dev Biol. 2021;9:664168.
1081 67. Embree MC, Chen M, Pylawka S, Kong D, Iwaoka GM, Kalajzic I, et al. Exploiting
1082 endogenous fibrocartilage stem cells to regenerate cartilage and repair joint injury. Nat
1083 Commun. 2016;7:13073.
1084 68. Jiang C, Centonze A, Song Y, Chrisnandy A, Tika E, Rezakhani S, et al. Collagen signaling
1085 and matrix stiffness regulate multipotency in glandular epithelial stem cells in mice. Nat
1086 Commun. 2024;15(1):10482.
1087 69. Khurana S, Schouteden S, Manesia JK, Santamaria-Martinez A, Huelsken J, Lacy-Hulbert
1088 A, et al. Outside-in integrin signalling regulates haematopoietic stem cell function via
1089 Periostin-Itgav axis. Nat Commun. 2016;7:13500.
1090 70. Damerau A, Rosenow E, Alkhoury D, Buttgereit F, Gaber T. Fibrotic pathways and
1091 fibroblast-like synoviocyte phenotypes in osteoarthritis. Front Immunol. 2024;15:1385006.
1092 71. Zhang F, Clair AJ, Dankert JF, Lee YJ, Campbell KA, Kirsch T. Cytokine Receptor-like
1093 Factor 1 (CRLF1) and Its Role in Osteochondral Repair. Cells. 2024;13(9).
1094 72. Primmer CR, Papakostas S, Leder EH, Davis MJ, Ragan MA. Annotated genes and
1095 nonannotated genomes: cross-species use of Gene Ontology in ecology and evolution
1096 research. Mol Ecol. 2013;22(12):3216-41.
1097 73. Wallis JW, Aerts J, Groenen MA, Crooijmans RP, Layman D, Graves TA, et al. A physical
1098 map of the chicken genome. Nature. 2004;432(7018):761-4.

1099